NASA Technical Memorandum 78741

(NASA-TM-78741) A BRIEF SURVEY OF ROTARY WING INDUCED-VELOCITY THEORY (NASA) 67 p HC A03/MF A01 CSCL 01A

N78-27085

Unclas
G3/02 25218

A BRIEF SURVEY OF ROTARY WING INDUCED-VELOCITY THEORY

HARRY H. HEYSON

JUNE 1978

National Aeronautics and Space Administration

Langley Research Center
Hampton, Virginia 23665

A BRIEF SURVEY OF ROTARY WING INDUCED-VELOCITY THEORY

by Harry H. Heyson

Langley Research Center
Hampton, Virginia 23665

SUMMARY

The development of rotary wing induced-velocity theory is traced from its origin as a momentum-theory estimate of average interference, through simple vortex theory, to its present status where it is indispensible in calculating blade loads. Applications to a variety of interference problems is demonstrated. Wherever possible, experimental results are presented to confirm the theory.

INTRODUCTION

All aerodynamic lifting devices, including helicopter and autogyro rotors, obtain their lift as the reaction from pushing air downward. The momentum thus imparted to the air sets up an induced field which interacts or interferes to a significant degree with anything placed near the lifting system; indeed, it interferes with the lifting system itself.

In the case of a helicopter rotor, the velocities induced by the field influence the forces on the blades as they rotate; they alter the effectiveness of tail surfaces; and they have powerful influences on the interference with the additional lifting devices used on a multitude of convertiplane designs.

The detail in which the induced flow must be known varies with the intended application. A gross overall average velocity through the rotor is adequate for many performance problems. The spacial, time-averaged, field is often adequate to predict tail effectiveness or mutual interference with other lifting systems. If detailed load distributions over the blades are required, an equally detailed knowledge of the instantaneous induced velocities along the blades is required. The difficulty encountered in obtaining the required information is more than proportional to the detail required in the velocities. In the simplest cases, the calculation is in closed form and occupies three or four lines. In the more difficult cases, the calculations may exceed the capacity of some of the largest digital computers.

The present paper attempts to summarize the state of knowledge of rotary-wing flow fields. It begins with the simple momentum methods applied to the rotor by Glauert. It then turns to the time-averaged flow field, where the first truly usable results were obtained by Walter Castles of Georgia Tech. The extension of Castle's work by NACA and a comparison of the theory with flow measurements are presented. Finally, the modern efforts toward using more detailed digital methods to obtain blade-load distributions are described.

In most cases, figures and equations presented herein, have been abstracted from the original reports. The notation, which varied from author to author, is, therefore, not consistent throughout this paper. It is hoped that the notes presented with equations, and the general context of the discussion, will suffice to allow the reader to infer the proper meanings for the symbols throughout the development.

DISCUSSION

MOMENTUM THEORY - THE AVERAGE INDUCED VELOCITY

Glauert (ref. 1), in the early 1920's, began the development of rotary wing blade-element theory. It was clear from analogous work on propellers and wings that the local angles of attack could not be found solely from geometric considerations. There must be an interference, or induced, velocity which resulted from the lift, and which entered into the angle of attack equations. No theory of the time predicted this induced velocity; however, the Froud momentum theory for propellers in static thrust resulted in

$$T = -\rho\pi R^2 w_0 (2w_0) \tag{1}$$

where T is the thrust, ρ the mass density of the fluid, R the radius, and w_0 the induced velocity through the disk (positive upward for a rotor). On the other hand, for a wing having a span of $2R$, it was known that the lift L was given by

$$L = -\rho\pi R^2 V(2w_0) \tag{2}$$

Glauert noted that these two expressions could be combined in a continuous fashion if the total velocity through the rotor disk was taken as the vector sum of the induced and forward velocities; that is, if $T \approx L$

$$T = -\rho\pi R^2 V_R(2w_0) \tag{3}$$

where V_R is the absolute value of the sum of the induced and forward velocities. He applied the resulting value of w_0 as a uniform induced velocity, or downwash, over the entire rotor disk. In terms of present rotor notation, where the thrust coefficient is

$$C_T = \frac{T}{\rho\pi R^2 (\Omega R)^2} \tag{4}$$

the inflow ratio (velocity ratio normal to the disk) is

$$\lambda = \frac{V\sin\alpha + w_0}{\Omega R} \tag{5}$$

and the advance ratio (velocity ratio parallel to the disk) is

$$\mu = \frac{V\cos\alpha}{\Omega R} \tag{6}$$

equation (3) may be expressed as

$$W_0 = -\frac{1}{2}\frac{C_T \Omega R}{\sqrt{\mu^2 + \lambda^2}} \tag{7}$$

Here the matter rested for about 25 years. Within the usable performance range of the machines of those days, such a simple theory was reasonably adequate. The first advances in rotor flow-field theory were not really occasioned by great known inadequacies in rotor theory as such - rather, it was the need to estimate downwash angles at the wings and tails of unloaded rotor configurations. For these purposes, simple momentum concepts were totally inadequate, and it was necessary to turn to at least a rudimentary vortex theory or its equivalent.

SIMPLE VORTEX THEORY

Work on a simple vortex theory for rotors was begun during World War II by Coleman, Feingold, and Stempin (ref. 2); however, it was an additional ten years before this work was brought into full flower by Castles and De Leeuw (ref. 3). (A mathematically different, but physically identical study was done in England by Mangler and Squire (ref. 4)).

The Vortex Model

The first step in setting up a simple vortex model is to choose a vortex pattern that is reasonably adequate on a physical basis and, at the same time, sufficiently simple that numerical results can be extracted. The wake of a rotor is more complicated than that of a wing, and a more involved model is required. If one examines a single-bladed rotor, as in figure 1(a), there would be a bound vortex along the blade. At the root, the free vortex is carried downward by the flow through the rotor and rearward by the flow past the rotor. The tip vortex is carried off in the same manner, but it also is affected by the rotation of the rotor; thus, it lies on a spiral path as shown.

Even this simple spiral is difficult to deal with so the next step is to divide the wake vortices into their axial and circumferential components and to discard the axial components as being of secondary importance. The wake then appears as a skewed stack of vortex rings as in figure 1(b). The final step is to assume that the rings are spaced so closely that they are equivalent to a continuous elliptic cylinder of vorticity as shown in figure 1(c).

The Induced Velocities

The induced velocities constituting the rotor field may then be found by integrating the Biot-Savart law over the entire wake. This can be accomplished in several manners. The development presented herein follows that of reference 5. The induced velocity of an element in the wake (fig. 2) is

$$d\bar{q} = \frac{1}{4\pi}\frac{d\Gamma}{dL}\frac{d\bar{s}\times\bar{a}}{|\bar{a}|^3}\,dL \tag{8}$$

where $\bar{q}$ is the induced velocity vector, L is the length along the wake, and $D\Gamma/dL$ is the vortex density (or vorticity) along the edge of the wake.

From figure 2, $\bar{s}$ and $\bar{a}$, are found to be

$$\bar{s} = \bar{i}(R\cos\psi+L\sin\chi) + \bar{j}(R\sin\psi) + \bar{k}(-L\cos\chi)$$

$$\bar{a} = \bar{i}(R\cos\psi+L\sin\chi-x) + \bar{j}(R\sin\psi-y) + \bar{k}(-L\cos\chi-z)$$

and $d\bar{s}$ is found by differentiating $\bar{s}$ with respect to ψ

$$d\bar{s} = \left[\bar{i}(-\sin\psi) + \bar{j}(\cos\psi) + \bar{k}(0)\right]R\,d\psi$$

Substituting these values into equation (8) yields

$$\bar{q} = \frac{R}{4\pi}\frac{d\Gamma}{dL}\int_0^{2\pi}\int_0^{\infty}\frac{\begin{vmatrix}\bar{i} & \bar{j} & \bar{k}\\ -\sin\psi & \cos\psi & 0\\ (R\cos\psi+L\sin\chi-z) & (R\sin\psi-y) & (-L\cos\chi-z)\end{vmatrix}\,dL\,d\psi}{\left[(R\cos\psi+L\sin\chi-z)^2 + (R\sin\psi-y)^2 + (-L\cos\chi-z)^2\right]^{\frac{3}{2}}} \tag{9}$$

For the moment, we will be interested only in the $\bar{k}$ (or w) component of induced velocity since this component is perpendicular to the disk. From equation (9)

$$w = \frac{R}{4\pi}\frac{d\Gamma}{dL}\int_0^{2\pi}\int_0^{\infty}\frac{(x\cos\psi+y\sin\psi-R-L\sin\chi\cos\psi)\,dL\,d\psi}{\left[R^2+x^2+y^2+z^2-2R(x\cos\psi+y\sin\psi) + 2L(z\cos\chi-x\sin\chi+R\sin\chi\cos\psi) + L^2\right]^{\frac{3}{2}}} \tag{10}$$

The integration with respect to L is not difficult and the forms will be found in tables of integrals. After substituting limits and the nondimensionalizing, the result is

$$w = \frac{-1}{4\pi} \frac{d\Gamma}{dL} \int_0^{2\pi} \frac{\left[1 - \left(\frac{x}{R}\cos\psi + \frac{y}{R}\sin\psi\right) + \frac{R_c}{R}\sin\chi\cos\psi\right]}{\left[\frac{R_c}{R} + \left(\cos\psi - \frac{x}{R}\right)\sin\chi + \frac{z}{R}\cos\chi\right]\frac{R_c}{R}} d\psi \qquad (11)$$

where R_c, the distance from the point (x,y,z) to the edge of the disk at ψ, is

$$R_c = \sqrt{R^2 + x^2 + y^2 + z^2 - 2R(x\cos\psi + y\sin\psi)} \qquad (12)$$

Equation (11) is not integrable, in general, except in terms of elliptic integrals of the third kind, and it is simpler to evaluate it numerically in a digital computer. One case which can be integrated is when (x,y,z) is at the center of the rotor ($x = y = z = 0$, $R_c = R$) for which equation (11) reduces to

$$w_0 = \frac{1}{4\pi} \frac{d\Gamma}{dL} \int_0^{2\pi} d\psi = -\frac{1}{2} \frac{d\Gamma}{dL}$$

The nondimensional induced velocity is obtained by dividing equation (11) by equation (12) to yield

$$\frac{w}{w_0} = \frac{1}{2\pi} \int_0^{2\pi} \frac{\left[1 - \left(\frac{x}{R}\cos\psi + \frac{y}{R}\sin\psi\right) + \frac{R_c}{R}\sin\chi\cos\psi\right]}{\left[\frac{R_c}{R} + \left(\cos\psi - \frac{x}{R}\right)\sin\chi + \frac{z}{R}\cos\chi\right]\frac{R_c}{R}} d\psi \qquad (13)$$

Local values of the induced velocity ratios may be obtained by numerical evaluation of equation (13). Charts of the induced velocities are available from which approximate values may be obtained. A collection of such charts is

given in reference 6. A sample set of charts (from ref. 7) for both the vertical and longitudinal induced velocity ratios is given in figure 3.

The Average Induced Velocity

As noted earlier, Glauert's formulation of the induced velocity of a rotor was merely a plausible guess. The simple vortex theory can be used to examine the validity of the value which he selected. Consider a rotor of b blades, each of which has a bound circulation of Γ over its entire length. The elemental lift on the blade is found from the Kutta-Joukowski theorem to be

$$dT = \rho U_T \Gamma dr \tag{14}$$

where U_T is the tangential velocity normal to the blade axis and Γ is the bound circulation. The total thrust of the rotor is found by integrating the elemental thrust over the length (radius) of the blades and then averaging this value around the disk; that is

$$T = \frac{b}{2\pi} \int_0^{2\pi} \int_0^R \rho \, (\Omega r + \mu \Omega R \sin\psi) \, \Gamma dr d\psi = \frac{1}{2} b \rho \Omega R^2 \Gamma \tag{15}$$

Substitute equation (15) into equation (4) to obtain

$$C_T = \frac{b\Gamma}{2\pi R^2 \Omega} \tag{16}$$

and then solve equation (16) for Γ to yield

$$\Gamma = \frac{2\Omega\pi R^2 C_T}{b} \tag{17}$$

Now the number of "vortex rings" formed per unit time at the rotor is $B\Omega/2\pi$. These are carried down the wake with the mean velocity at the rotor $(\Omega R\sqrt{\mu^2 + \lambda^2})$. Thus, the vorticity along the edge of the wake is

$$\frac{d\Gamma}{dL} = \frac{\Gamma \frac{b\Omega}{2\pi}}{\Omega R \sqrt{\mu^2 + \lambda^2}} \tag{18}$$

Substitute equation (17) into equation (18), and simplify the result to yield

$$\frac{d\Gamma}{dL} = \frac{\Omega R C_T}{\sqrt{\mu^2 + \lambda^2}} \tag{19}$$

Simple vortex theory gives the induced velocity at the center of the rotor as equation (12). Substitute equation (19) into equation (12) to obtain

$$w_0 = -\frac{1}{2}\frac{\Omega R C_T}{\sqrt{\mu^2 + \lambda^2}} \tag{20}$$

Equation (20) for the center of the rotor is identical to Glauert's result (eq (7)) for the average over the entire rotor. The induced velocity varies widely over the rotor disk; however, reference 8 has shown that, even when harmonic variations in Γ occur at the blades, the value at the center is identically equal to the average value. Thus, the simple vortex theory confirms the momentum theory formulated by Glauert.

VORTEX THEORY FOR NONUNIFORM AXISYMMETRIC DISK LOADING

At this point, only blades of constant circulation Γ have been considered. For such a blade, the radial gradient of blade loading is obtained by taking $U_T = \Omega r$ and reforming equation (14) to obtain

$$\frac{dT}{dr} = \rho \Omega r \Gamma \tag{21}$$

Equation (21) shows that, for uniform bound circulation, the thrust per unit length of blade varies linearly from zero at the root to a maximum at the tip. Now consider the thrust per unit area of the swept disk. The area of an annulus of radial width dr is $2\pi r dr$. Thus, the load per unit area on this annulus is (for b blades)

$$\frac{dT}{dA} = \frac{b\rho\Omega r \Gamma dr}{2\pi r dr} = \frac{b\rho\Omega\Gamma}{2\pi} \tag{22}$$

Thus, uniform circulation along the blades produces a uniform load per unit area on the swept disk. Because, the disk is circular, the spanwise distribution of lift viewed from behind the rotor is semicircular; that is, a special case of an elliptic spanwise load distribution - the ideal distribution for the minimum induced drag of a wing.

In general, the disk load distribution of a rotor is not uniform. If the radial distribution of induced velocity was neglected, a constant-chord untwisted blade would have a blade loading proportional to r^2 not r as in equation 20. Twist and taper further alter the load grading, and the cutout to provide the rotor hub is a nonuniformity in itself. Any practical rotor has zero disk-load distribution at its center.

In general, Γ is some function of r. Regardless of the actual variation chosen, equations (21) and (22) show that the disk load distribution will vary as $1/r$ times the blade load distribution. The flow field of nonuniformly loaded rotor disks can be obtained from the field of the uniformly loaded rotor disk provided that the disk load distribution required is axisymmetric (ref. 9).

Consider the triangular load distribution of figure 4. It can be approximated by a stepwise distribution of loads comprised of one large positive load (1.5 times normal strength) and a series of small negative loads of smaller radius. Such a load distribution would be generated by a nest of coaxial vortex cylinders such as shown in figure 5.

The contribution of each of these cylinders to the flow at (X/R, Y/R, Z/R) will be proportional to its vortex strength and can be read from charts such as figure 3 at the point $[(X/R)(R/R_V), (Y/R)(R/R_V), (Z/R)(R/R_V)]$. The induced velocity at that point is the sum of the contributions of all the cylinders. A sample calculation for a triangular loading at (X/R = 0.2, Y/R = 0, Z/R = 0.1) and for $\chi = 90^0$ is shown in figure 4.

The actual distribution of load on the disk has very large and significant effects on the distribution of induced velocity. A few sample charts are presented in figure 6. A direct comparison is presented in figure 7. Observe that there is a region of upwash in front of, and encompassing, the leading edge of the disk in each case. The major differences occur over the disk and across the wake. In constrast to the smooth increase in downwash along the rotor axis in the uniform case, the triangular case shows an increase at first, then a decrease to zero at the rotor center, an upwash behind the center, and then, finally a rapid increase to the trailing edge. The distribution across the wake itself is markedly different in both cases.

One other point is very significant. Under the present assumptions, the rotor-induced flow is dependent only upon the skew angle χ. The total flow field is the vectorial sum of the uniform external flow and the rotor induced velocities. The total field may be markedly different dependent upon the rotor angle of attack and loading. This feature is illustrated by figure 8.

COMPARISON WITH EXPERIMENT

NACA Rep 1319 (ref. 9) presents the results of comprehensive flow surveys near a rotor operating in the wind tunnel. Sample results are given in figures 9 and 10. Comparison of theory and experiment in the central plane of the rotor is shown in figure 11. It is evident that the radial distribution of loading is significant in the correlation. On the other hand, an earlier paper (ref. 10) showed that the uniform load distribution does give a reasonably good approximation to the average induced velocity across a span equal to the rotor diameter.

Another significant feature of figure 11 is the evident failure of the theory in the region aft of the rotor. This result is obtained because of the extremely rapid roll up of the wake vorticity behind the rotor. Figure 12 shows contours of equal vorticity behind the rotor and it is evident that the roll up is already well underway at the trailing edge of the rotor. In this region, the wake can be modeled by assuming it to be about the same as that behind a wing of equal span.

Some Applications of the Theory

Wind tunnel flow measurements give reason to believe that the major factors affecting the flow field are included in the theoretical considerations described above. Thus, the theoretical results should be adequate to explain the induced effects found on helicopters and compound aircraft (ref. 11). This section of this paper will examine the extent to which this conclusion is true.

Multirotor helicopters.- The first example will be a tandem-rotor system which was tested in the Langley full-scale tunnel (ref. 12). Basically the model was simply two identical 15-foot-diameter rotors with no vertical offset and a gap of only 6 inches between the rotor tips. Thrust and torque were measured and, in addition, flow surveys (ref. 10) were made at locations very near to the rotor. For one level-flight condition, the flow measurements are shown in figure 13. The data points represent the average induced velocity across a span of one rotor diameter. These points indicate that the average induced velocity through the rear rotor was three times that through the front rotor. This corresponds with the simultaneous power measurements which indicated that the rear rotor required three times as much induced power as the front rotor.

The calculated induced velocities in this case are also shown on figure 13. These calculated curves are very close to the measured flow data and indicate that the rear rotor should require more than 2.8 times as much induced power as the front rotor. Thus it appears that the theory should be adequate for estimating the effect of interference on the overall performance of multirotor helicopters. There are, however, certain reservations to this conclusion which will be discussed in a later section.

Rotor-wing interference.- Recent attempts to combine the forward-flight capability of an airplane with the vertical-flight capability of a helicopter have led to a number of unloaded-rotor convertiplane designs. Generally speaking, these compound aircraft are characterized by the presence of a rotor and a wing operating in close proximity to each other. Some degree of mutual interference is bound to be present and it may have a major effect upon the overall performance of the aircraft.

Two such machines are shown in figure 14. These are the PCA-2 autogyro and the XV-1 convertiplane. If the hovering ability of the XV-1 is neglected, the two aircraft are remarkably similar despite the passage of some twenty-five years between their designs. No power is applied to the rotor in forward flight since both operate as autogyros in this flight regime. An auxiliary wing is provided, and this wing carries a large portion of the lift. The propulsive force is obtained in each case by means of a propeller. The major differences between the two aircraft lie in both the absolute and the relative loadings of the wing and the rotor.

The PCA-2 autogyro was tested in flight. The wing load was determined by measuring the pressures on the wing surfaces. The remainder of the gross weight is supported by the rotor. Thus the performance is relatively simple to compute since the rotor lift coefficient and, consequently, its mean, or momentum theory,

value of induced velocity are already known. The induced velocity at the wing due to the rotor is then taken from the charts. Adding this induced velocity vectorially to the free-stream velocity yields the direction of flow at the wing and the effective wing angle of attack. The lift of the wing can then be determined from the isolated wing characteristics.

Figure 15 compares the wing load in percent of the total lift as calculated by the foregoing procedure and as measured in gliding flight. (If the powered-flight conditions had been chosen it would, of course, have been necessary to correct the wing lift for the increased dynamic pressure in the slipstream propeller.) At each tip-speed ratio, the measured load is represented by a circle and the calculated load is represented by a square. The agreement is good, the maximum error being about 6 percent.

The XV-1 convertiplane was tested in the Ames full-scale tunnel and, because of the manner in which the tests were conducted, presents a much more interesting problem. During the tests, the performance of the rotor, the convertiplane without its rotor, and the complete convertiplane were all measured separately. The results are shown in figure 16, where the symbols indicate the measured lift and drag coefficients which are based in all cases on the rotor disk area. The sum of the "rotor only" data and the "rotor off" data is given by the broken line. The difference between this line and the data for the complete configuration is large and may be charged almost entirely to interference.

The calculation in this case depends upon a knowledge of the total lift required, just as it does in a flight calculation. At each angle of attack, the rotor is assumed to have its "isolated" lift. Then the wake skew angle is computed and the induced velocity at the wing is determined. This induced velocity is used to determine the effective angle of attack and lift of the wing. The sum of rotor lift and wing lift, in general, is not the correct lift. The lift of the rotor is altered to correct the overall configuration lift, and the procedure is repeated iteratively until the total configuration lift is obtained. The process is rapidly convergent in a practical sense. Once the lift coefficients of both the rotor and the wing are determined, it is a simple matter to determine their drag coefficients.

The results of such calculations are shown as the solid curves of figure 16. The accuracy of the procedure is attested by the remarkably close agreement with the observed performance of the complete configuration.

Tail Surfaces.- Figure 17 presents the downwash measured from the floating tail of the XV-1. Similar measurements obtained from an 8/31 scale model in the return passage of the WADC 20-foot tunnel are also shown.

The induced angle at the tail is affected by both the wing and the rotor. The lift coefficients obtained from the rotor-wing interference calculations were used for determining the contribution of each to the downwash angle at the

tail. The calculated results are shown in figure 17 for the cases of uniform and triangular loading. It should be noted that the span of the tail is approximately one-half radius. Thus this case corresponds to neither the one-diameter span required by the uniformly loaded rotor induced-velocity chart nor the zero span required by the triangularly loaded rotor chart. Therefore, the data should fall between the two calculated curves, and this is exactly the result shown in figure 17.

The degree of agreement shown here can be expected only when the rotor lift coefficient is low. If it were much higher the flow would roll up faster and might cause large errors. For the case of large lift coefficients, the downwash angles may be calculated fairly well be assuming that the flow is similar to that of the uniformly loaded wing.

Aerodynamic loading of rotor blades.- One of the most troublesome features of rotary-wing aircraft is the large magnitude of the fluctuating aerodynamic loads on the rotor blades. These loads have been measured during wind-tunnel tests of rotors equipped with instrumentation capable of measuring the instantaneous pressure distribution on the blades. Figure 18 shows the aerodynamic loading at the three-quarter-radius station as measured during one of these tests (ref. 13). It may be seen that in this case the loading fluctuates with an amplitude of about one-half of the mean load. Needless to say, the stresses resulting from fluctuating loads of this magnitude could easily represent the critical design condition for the rotor.

The data shown in figure 18 was obtained at a tip-speed ratio of only 0.08. At this speed, the older blade-element theory with uniform inflow indicates that the aerodynamic load should be essentially constant. This, in itself, is not too disturbing since it is generally recognized that the assumption of uniform induced velocity inherent in the theory limits it to computing only the overall performance rather than the detailed blade loading.

The blade-element theory should, of course, yield a much more accurate estimate of the blade loading if the correct induced velocity were used. In order to find just what this induced velocity should be, one investigation took the measured blade loading, inserted it into blade-element theory, and worked backwards through the theory to obtain an effective induced velocity. The results are shown in figure 19 where they are compared with the theoretical induced velocities. It is immediately evident that there is no correlation at all between the required induced velocity and the theoretical induced velocity. Even the trends are completely reversed in some locations. Thus it appears that the calculated induced velocities cannot lead to the correct blade loading.

Reexamination of basic concepts.- The complete failure of the induced flow theory in the blade-load problem is in sharp contrast with its success in computing interference effects. The reason for this failure is very basic and may be explained by returning to the original concept of the rotor wake as a spiral vortex (fig. 20). As pointed out previously, this spiral will move downward with time and the actual induced flow will be a function of time. This time-dependency was lost as a direct result of the simplifications adopted for the analysis. The calculated induced velocity is therefore a time-averaged value of the actual induced velocity.

Now consider a point P , fixed in its position with respect to the rotor, as, for example, a point on a fixed-wing surface. As the spiral vortex progresses downward, the point P will "see" all of its possible positions. Therefore, the mean induced velocity at P should be the time-averaged value calculated by theory. Thus, the calculated induced velocities allow accurate estimates of rotor-wing interference to be made.

Next consider point Q which is on the rotor blade and which rotates with the blade. Since the spiral vortex starts at the blade tip, there will, at any azimuth position, be one, and only one, position of the spiral with respect to Q . Thus Q will not "see" the time-averaged induced velocity given by the theory. Thus, as shown before, the theory cannot be applied to finding the induced velocities needed for calculating the blade loads. The actual blade loading problem is closely related to flutter in that the unsteady aerodynamics cannot be neglected.

The more modern rotor theories take into account the unsteady character of the flow and, in addition, turn to more refined models of the wake. A brief survey of some of the more recent developments in this area will follow.

There is an intermediate problem between the average external interference and the detailed blade loads. Consider the point R on a second rotor near the first. Does this point see a time-averaged velocity or not? Locally, on the blade, it probably does not, and the change in the detailed blade loading as a result of interference can probably not be calculated with any degree of accuracy. However, at least for the tandem rotors of NACA TN's 3236 (ref. 12) and 3242 (ref. 10), there is experimental evidence to indicate that the overall rotor forces can be determined by use of the present theory. This may not be the case for all configurations. It is therefore suggested that multirotor interference calculations based on the present induced-flow theory be accepted for the present but always subject to the provision that experimental verification is required in each case.

CALCULATION OF BLADE LOADS

The more modern applications of rotary wing vortex theory involve the calculation of the details of the blade load distribution. The discussion herein will largely follow the developments in the United States. Although complete details do not appear to be available in this country, Mil's textbook (ref. 14) makes it clear that very similar developments have taken place in the USSR and that those analyses often predated our own. The present discussion must also deal only in generalities. Closed form solutions to the problem do not exist. Only the numerical results from specific sample cases run on digital computers are available.

The earlier discussion has shown clearly that the instantaneous velocities, not the average velocities, at the blade are required. In addition, it is evident that quasi-static solutions can not be meaningful in the face of the widely varying local velocities and angles of attack on the blades. The need for an unsteady analysis was further shown by the essentially simultaneous papers

of Loewy (ref. 15) and Timmon and van de Vooren (ref. 16). Both analysis demonstrated the existence of previously uncalculated wake-excited flutter modes even for a hovering rotor.

The initial theoretical investigation of blade loads was conducted by Piziali and DuWaldt at Cornell Aero Labs (ref. 17). The model used for their calculations is shown in figure 21. The blade is divided into a number of radial segments with the bound vortex fixed on the quarter chord. The bound circulation along each radial segment is constant. Thus, at each junction of segments a vortex will be shed, and the strength of this vortex will be equal to the difference in circulation of the two segments. The rotational motion of the blade is considered in terms of a number of azimuth steps with the bound circulation changing from step to step. In order to satisfy conservation of vorticity, a vortex must be shed from, and parallel to, the trailing edge of the blade at each step. Furthermore, the strength of this vortex must be equal to the difference in bound circulation between the two azimuth steps at each radial station. This grid-like wake is assumed to be carried uniformly away from the rotor tip-path plane by the forward velocity and by a uniform average induced velocity. Thus, it is constrained to lie within the cylindrical boundaries of the wake model used earlier in the average downwash calculations.

At the start of the calculations, the bound circulations on the blade are unknown; however, all of the wake vortex strengths may be formed as functions of the unknown bound circulations. The blade angles, flapping angles, and the deformations of the blade were preassigned in this analysis; thus, the dynamic response of the blades was not calculated. Control points were specified on the three-quarter chord at the midpoint of each segment. It was then possible to set up an array of simultaneous equations in the unknown blade circulations, using the Biot-Savert law to obtain the induced velocities at the control points. These simultaneous equations were then solved by matrix inversion techniques on the computer.

Observe the interrelationships involved in the solution. Charts of induced velocities for standardized load distributions no longer have any meaning. The only distribution with meaning is the one for that particular rotor at that particular flight condition.

The results from the new technique were far superior to the old uniform-downwash, quasi-static theory in many respects; however, as pointed out by the authors, there were also numerous problems. One major problem was that the calculated first-harmonic flapping moment was not zero, even when measured blade motions and deformations were input to the program. It was further recognized that the single three-quarter-chord control point was probably too crude, and that wake deformations might have to be considered as well.

Certain of these improvements were incorporated by Piziali in a later paper (ref. 18). In this version of the analysis, the blade was represented as a continuous distribution of vorticity by means of a Glauert series and the spanwise vorticity behind the trailing edge was "effectively fitted" with a continuous sheet (ref. 19) in the region immediately behind the blade (fig. 22). The entire calculation was set up in a loop such that the airloads were computed and then the resulting flapping and blade bending were computed. These results

were compared with the same quantities from the previous iteration and the entire procedure was repeated until the airloads, flapping, and dynamic response all converged. A sample set of results is compared with flight measurements in figure 23. Considering the complexity of the calculation and the simplifying assumptions, the results were quite encouraging.

Piziali's discussion pointed to the fact that many of the remaining discrepancies between theory and experiment could be qualitatively accounted for by physically reasonable distortions of the wake from the simple helical sheets which he was still using. Actually, Crimi, also at Cornell Aero Lab, was already working on the problem.

Crimi's original analysis (ref. 20) was directed at the external field of the rotor, and, for this purpose, he represented the wake by a single tip vortex from each blade. No spanwise vorticity was used despite the assumption that the tip vorticies had a strength containing a sine ψ component. Rigid helices were assumed at the start of the calculation, and numerous control points were chosen along the helices. Then the induced velocities at the control points were calculated. (Certain infinites in the calculation were avoided by the assumption of finite vortex cores.) The vortices were then allowed to convect to a new position with these velocities over a time period equal to one step in blade azimuth position. The process was repeated with the new positions until further changes in the wake positions were insignificant. The final wake position could then be used to calculate the flow throughout the field.

The wake resulting from this calculation is shown in figure 24. It obviously duplicates, at least qualitatively, the wake distortions which were found earlier in the wind-tunnel flow measurements. A comparison of the time-averaged measured and calculated flow fields is shown in figure 25. Considering that Crimi's assumptions omit the effect of radial disk-load distribution, the agreement is very encouraging.

More recently, Sadler (refs. 20, 22) has incorporated similar wake distortions into the calculation of blade loads using a full vortex-mesh and working with the unsteady aerodynamic problem. The solution is aided by a "rotor start-up" approach; that is, the theoretical rotor commences from a dead start in which there is no wake at all. In the first time increment a short wake is shed, approximate blade loads are calculated, and the short wake is relocated. The process is repeated by steps in aximuth until the complete wake is generated. Samples of the results are presented in figures 26 to 31. Once more the results are encouraging.

It would be premature to claim that the problem of calculating blade loads is solved. The comparisons between theory and experiment still indicate uncomfortably large differences. On the other hand, it is evident that many of the necessary elements to a solution have been determined and the basic problems dealt with to some extent. It is clear that far more detail is required than has been employed to date. Unfortunately, this detail is very expensive in terms of computer storage requirements, running time, and cost.

CONCLUDING REMARKS

The development of rotary wing induced-velocity theory bas been traced from its origin as a momentum-theory estimate of average interference, through simple vortex theory, to its present status where it is indispensible in calculating blade loads. Applications to a variety of interference problems has been demonstrated. Wherever possible, experimental results have been presented to confirm the theory.

REFERENCES

1. Glauert, H.: A General Theory of the Autogyro. R&M No. 1111, British A.R.C., 1926.

2. Coleman, Robert P.; Feingold, Arnold M.; and Stempin, Carl. W.: Evaluation of the Induced-Velocity Field of an Idealized Helipcopter Rotor. NACA WR L-126, 1945. (Formerly NACA ARR L5E10.)

3. Castles, Walter Jr.; and De Leeuw, Jacob Henri: The Normal Component of Induced Velocity in the Vicinity of a Lifting Rotor and Some Examples of Its Application. NACA Rep. 1184, 1954. (Supercedes NACA TN 2912.).

4. Mangler, K. W.; and Squire, H. B.: The Induced Velocity Field of a Rotor R&M No. 2642, British A.R.C., 1950.

5. Heyson, Harry H.: Equations for the Induced Velocities Near a Lifting Rotor with Nonuniform Azimuthwise Vorticity Distribution. NASA TN D-394, 1960.

6. Jewel, Joseph W., Jr.; and Heyson, Harry H.: Charts of the Induced Velocities Near a Lifting Rotor. NASA Memo 4-15-59L, 1959.

7. Heyson, Harry H.: Theoretical and Experimental Investigation of the Performance of a Fan-In-Wing VTOL Configuration. NASA TN D-7498, 1973.

8. Heyson, Harry H.: A Note on the Mean Value of Induced Velocity for a Helicopter Rotor. NASA TN D-240, 1960.

9. Heyson, Harry H.; and Katzoff, S.: Induced Velocities Near a Lifting Rotor with Nonuniform Disk Loading. NASA Rep. 1319, 1957. (Supersedes NACA TN 3690 by Heyson and Katzoff and NACA TN 3691 by Heyson.).

10. Heyson, Harry H.: Preliminary Results from Flow-Field Measurements Around Single and Tandem Rotors in the Langley Full-Scale Tunnel. NACA TN 3242, 1954.

11. Heyson, Harry H.: Induced Flow Near a Rotor and Its Application to Helicopter Problems. Proceed. 14th Ann. Natl. Forum, Amer Helicopter Soc., April 16-19, 1958. (Also available as: Induced Flow Near a Helicopter Rotor. Aircraft Engineering, Vol. 31, No. 360, Feb. 1959, pp 40-44).

12. Dingeldein, Richard D.: Wind-Tunnel Studies of the Performance of Multirotor Configurations. NACA TN 3236, 1954.

13. Rabbott, John P., Jr.; and Churchill, Gary B.: Experimental Investigation of the Aerodynamic Loading on a Helicopter Rotor in Forward Flight. NACA RM L56I07, 1956.

14. Mil', M. L.; Nekrasov, A. V.; Braverman, A. S.; Grodko, L. N.; and Leykand, M. A.: Helicopters, Calculation and Design. Vol. I.- Aerodynamics, NASA TT F-494, 1967.

15. Loewy, R. G.: A Two-Dimensional Approximation to the Unsteady Aerodynamics of Rotary Wings. Jour. Aero. Sci., Vol. 24, No. 2, Feb. 1957, pp 81-92, 144.

16. Timmon, R.; and Van De Vooren, A. I.: Flutter of a Helicopter Rotor Rotating in Its Own Wake. Jour. Aero. Sci., Vol. 24, No. 9, Sept. 1957, pp 694-702.

17. Piziali, Raymond A.; and Du Waldt, Frank A.: A Method for Computing Rotary Wing Airload Distribution in Forward Flight. Trecom TR 62-44, 1962.

18. Piziali, Raymond A.: A Method for Predicting the Aerodynamic Loads and Dynamic Response of Rotor Blades. USAAVLABS TR 65-74, 1966.

19. Daughaday, H.; and Piziali, Raymond A.: An Improved Computational Model for Predicting the Unsteady Aerodynamic Loads of Rotor Blades. Jour. Amer. Helicopter Soc., Vol. 11, No. 4, Oct. 1966. pp 3-10.

20. Crimi, Peter: Prediction of Rotor Wake Flows. Cal. USAAVLABS Symposium on Aerodynamic Problems Associated with V/STOL Aircraft. Buffalo, N.Y., June 1966, Vol. I.

21. Sadler, S. Gene: Development and Application of a Method for Predicting Free Wake Positions and Resulting Rotor Blade Air Loads. Vol. I - Model and Results. NASA CR-1911, 1971 and Vol. II - Program Listings. NASA CR-1912, 1971.

22. Sadler, S. Gene: Main Rotor Free Wake Geometry Effects on Blade Air Loads and Response for Helicopters in Steady Maneuvers. Vol. I - Theoretical Formulation and Analysis of Results. NASA CR-2110, 1972. Vol. II - Program Listings, NASA CR-2111, 1972.

(a) Spiral wake. (b) Vortex ring wake. (c) Cylindrical wake.

Figure 1. - Assumed wake of rotor.

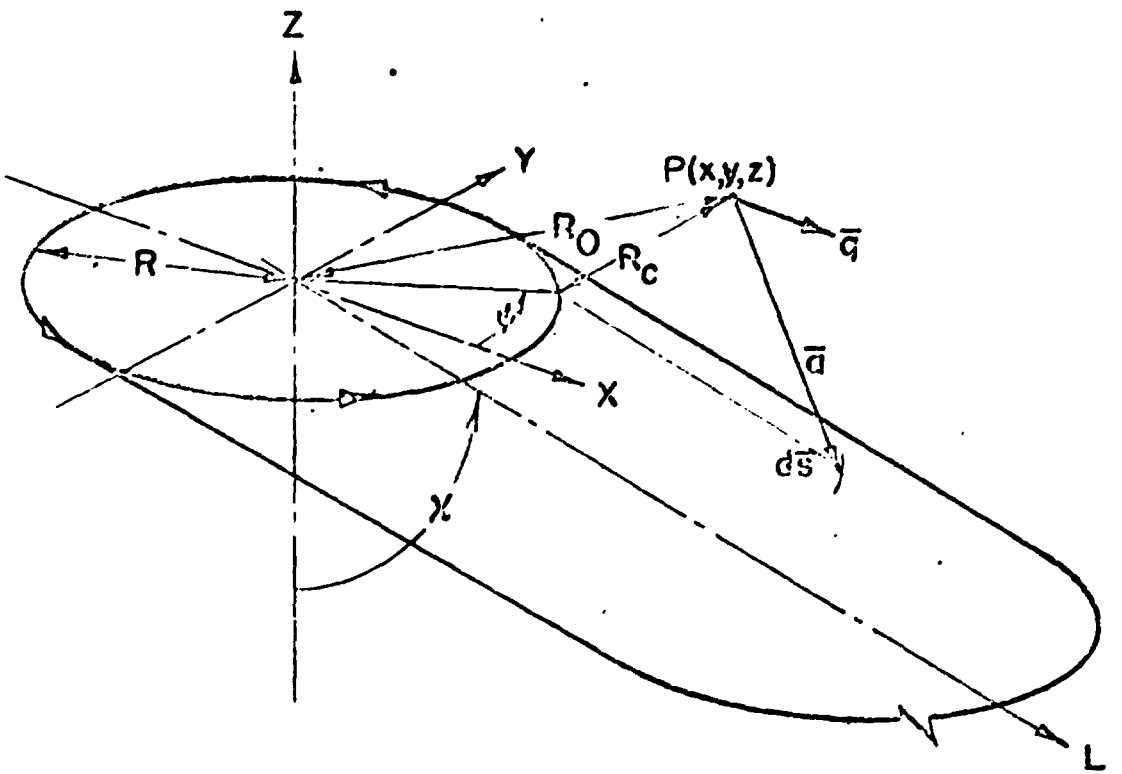

Figure 2. - Rotor wake system.

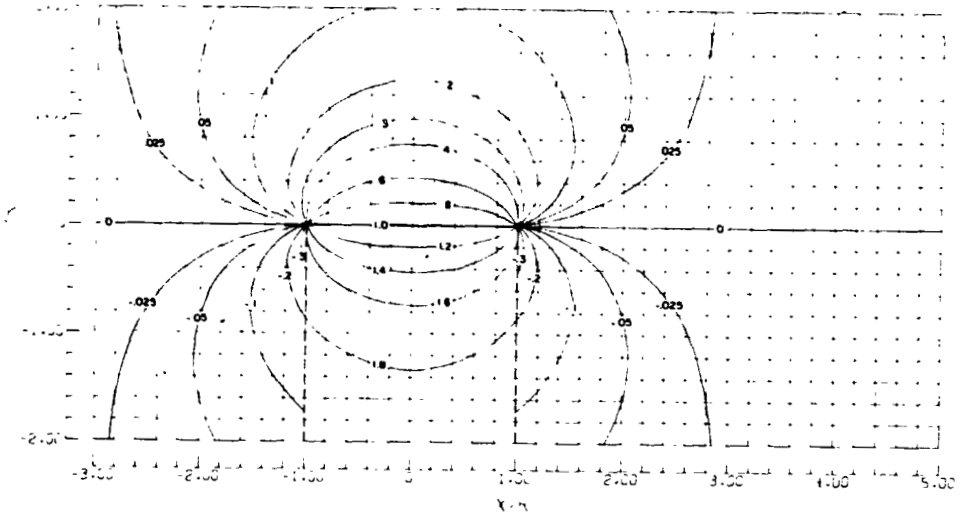

Contours of w/w_0

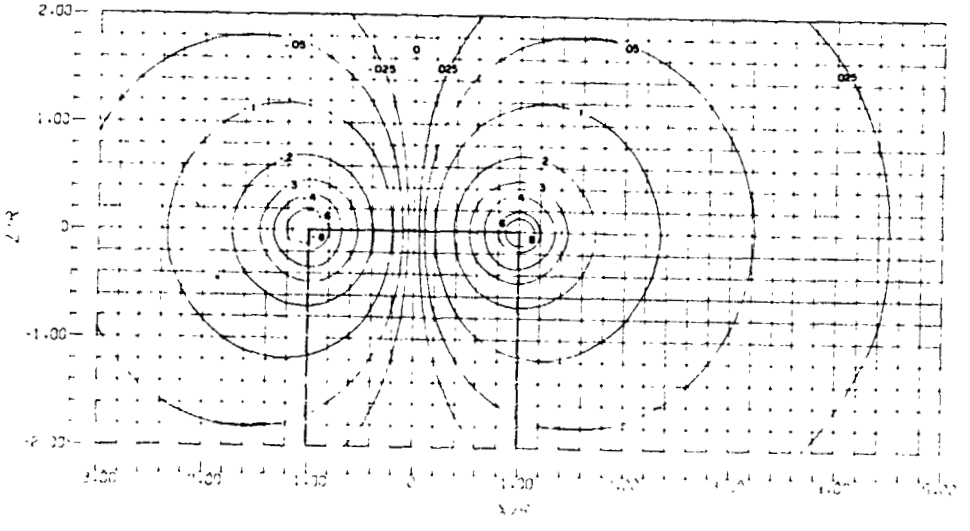

Contours of u/w_0
(a) $\chi = 0^0$

Figure 3. - Induced velocities in the central longitudinal plane of a rotor with uniform disk loading.

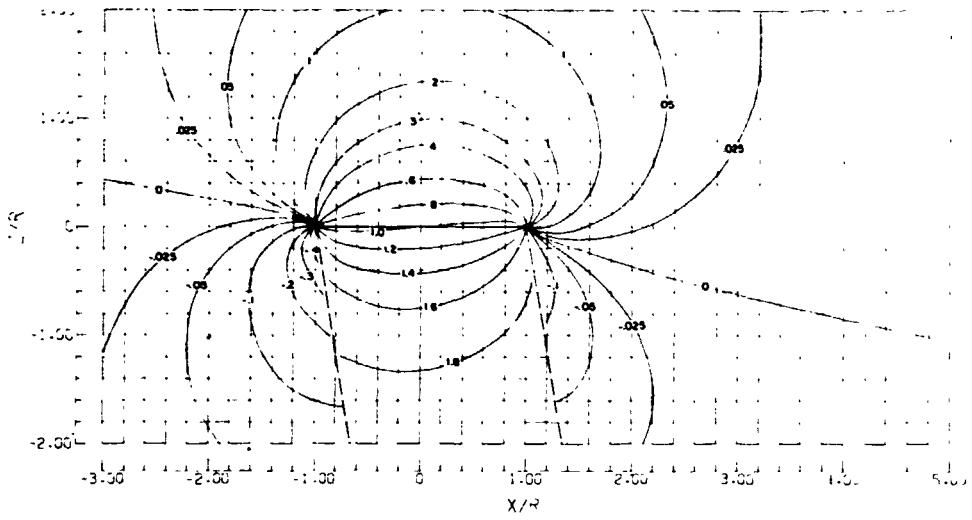

Contours of w/w_o

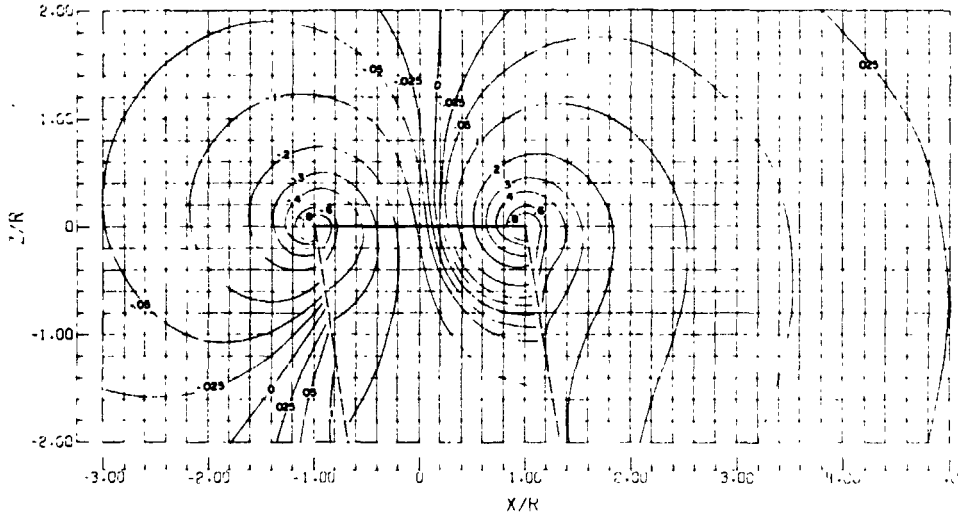

Contours of u/w_o
(b) $\chi = 10^o$

Figure 3. - Continued.

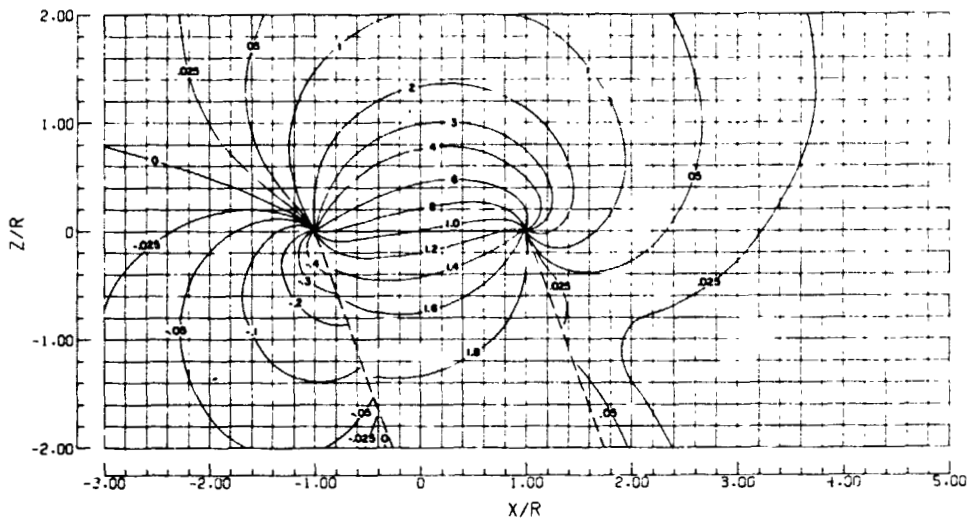

Contours of w/w_o

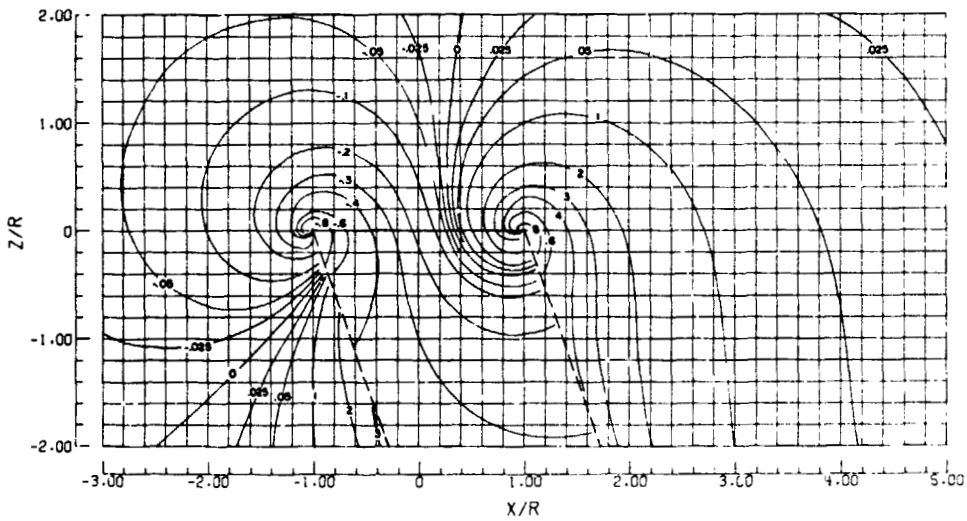

Contours of u/w_o
(c) $\chi = 20^o$

Figure 3. - Continued.

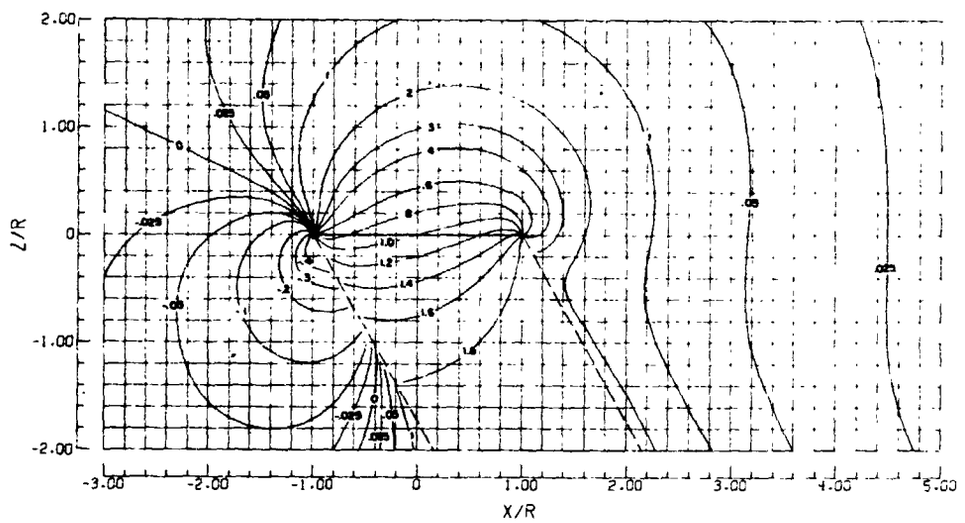

Contours of w/w_o

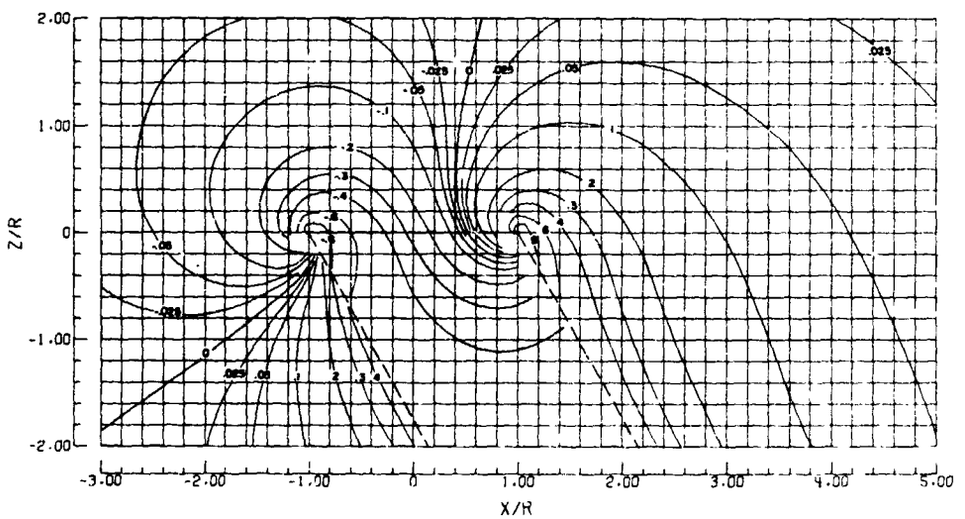

Contours of u/w_o
(d) $\chi = 30^o$
Figure 3. - Continued.

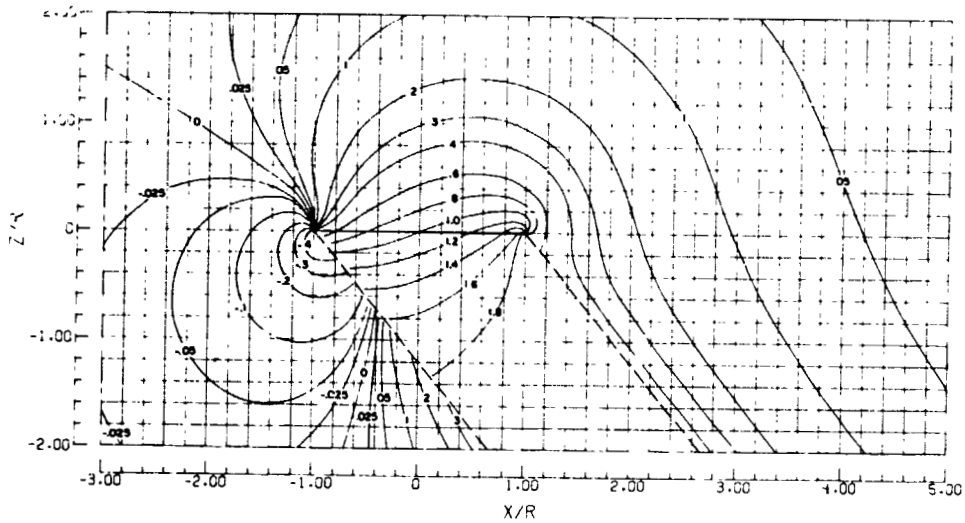

Contours of w/w_o

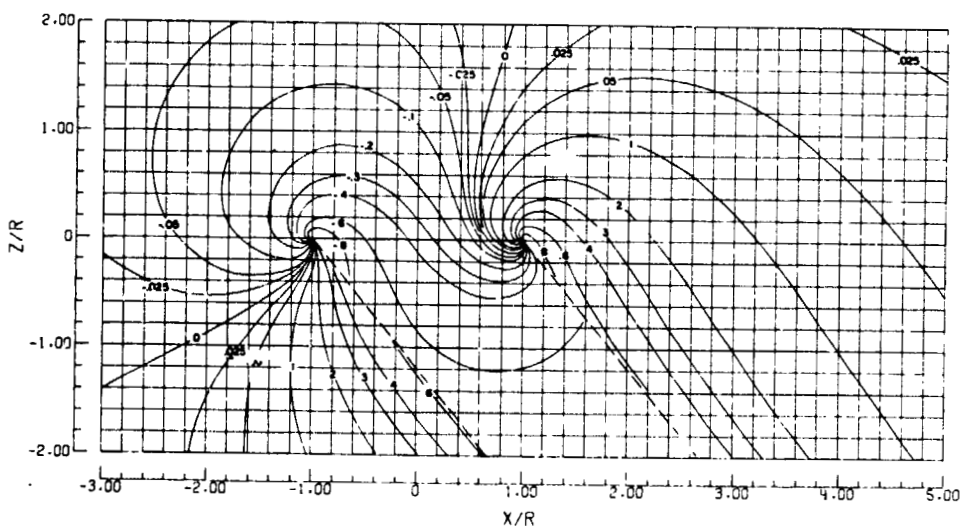

Contours of u/w_o
(e) $\chi = 40^o$

Figure 3. - Continued.

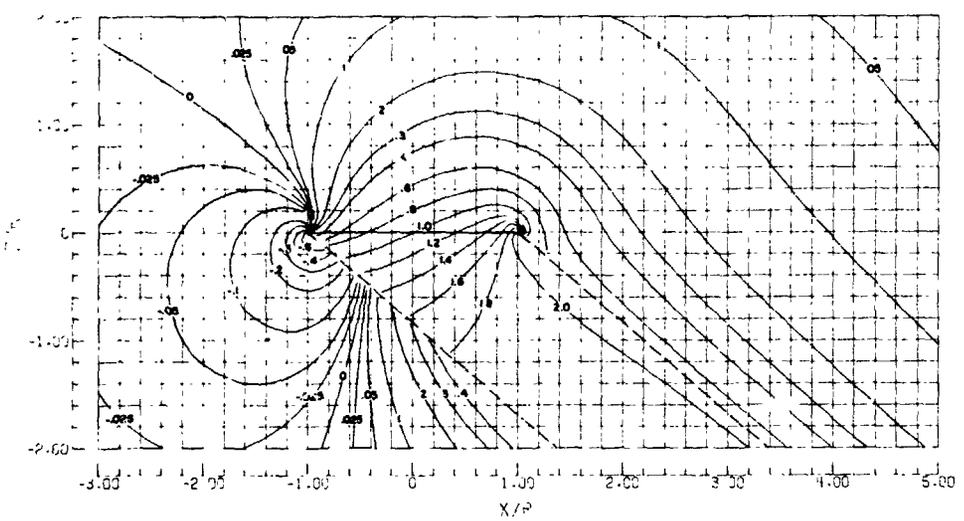

Contours of w/w_0

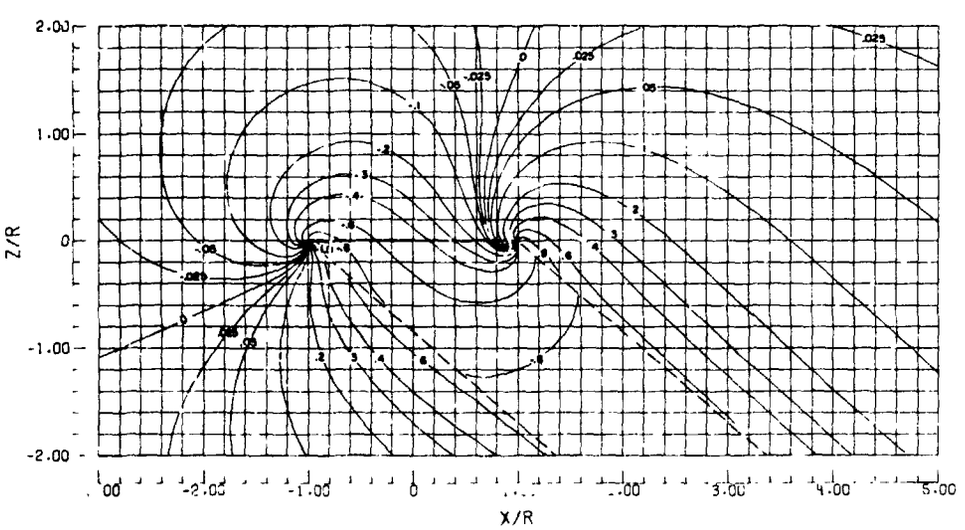

Contours of u/w_0
(f) $\chi = 50^0$

Figure 3. - Continued.

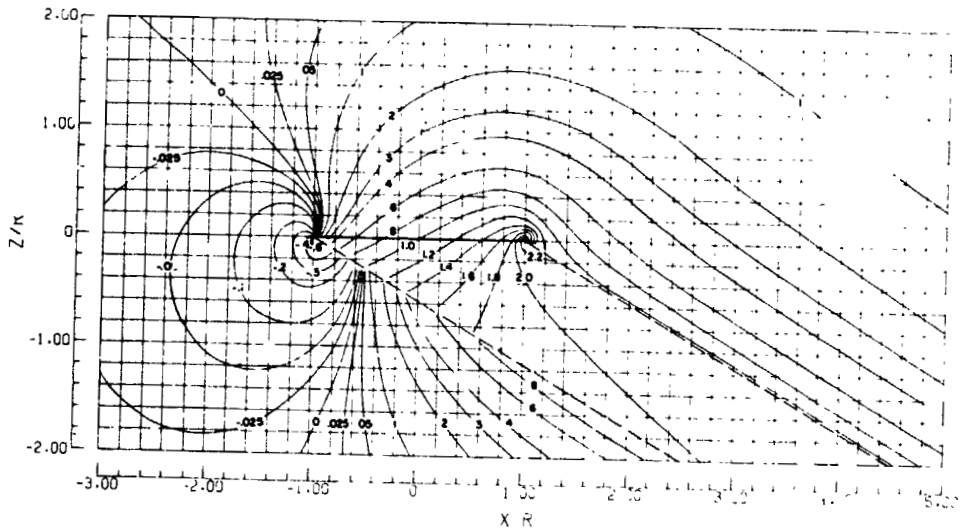

Contours of w/w_o

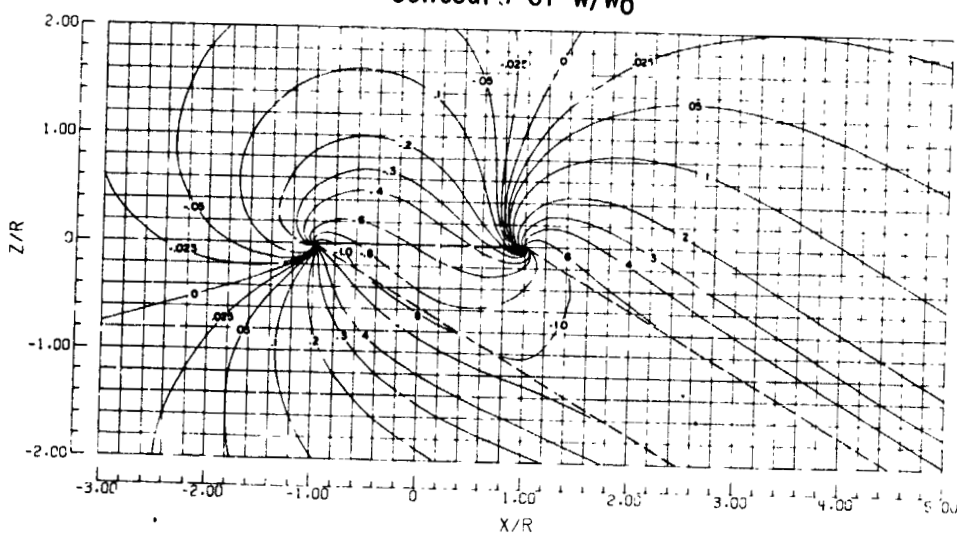

Contours of u/w_o
(g) $\chi = 60^o$

Figure 3. - Continued.

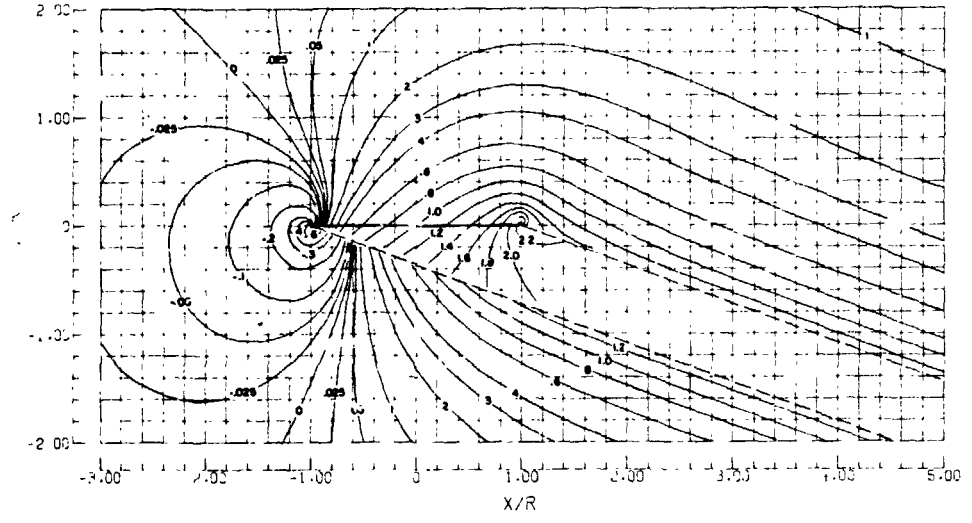

Contours of w/w_o

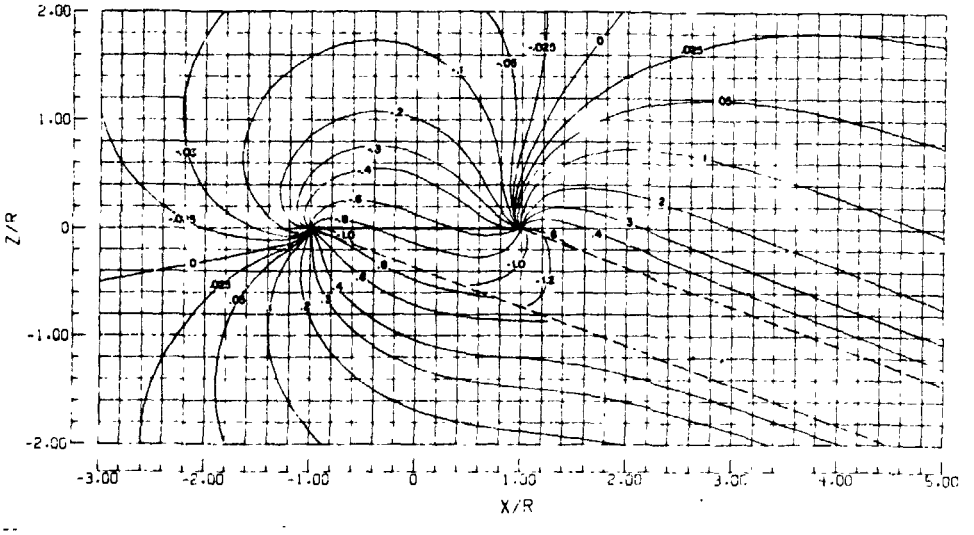

Contours of u/w_o
(h) $\chi = 70^o$

Figure 3. - Continued.

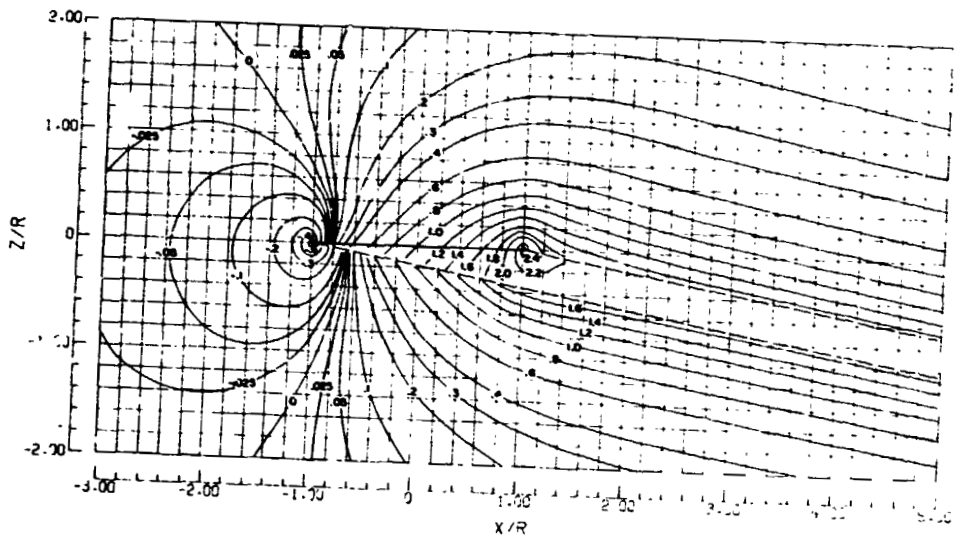

Contours of w/w_o

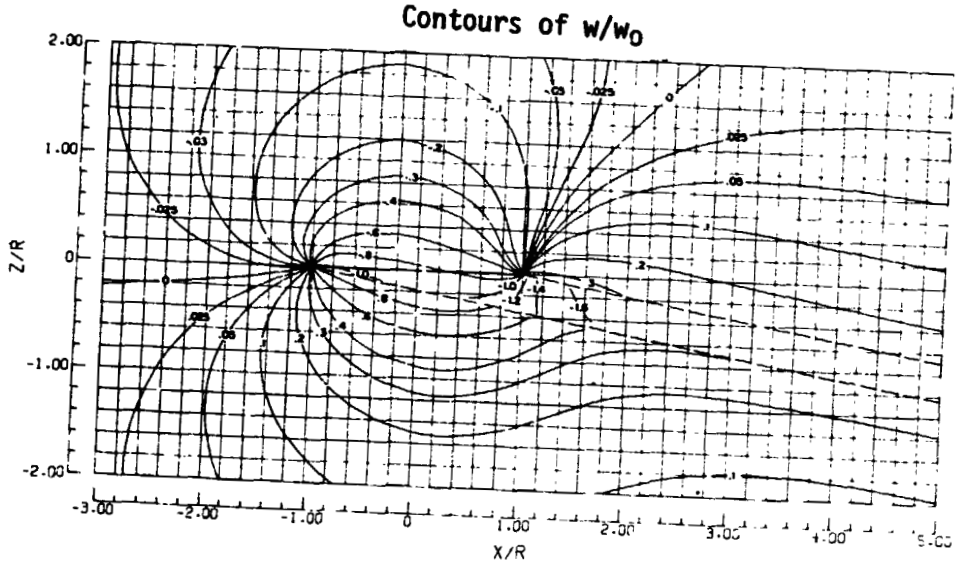

Contours of u/w_o
(i) $\chi = 80^o$
Figure . - Continued.

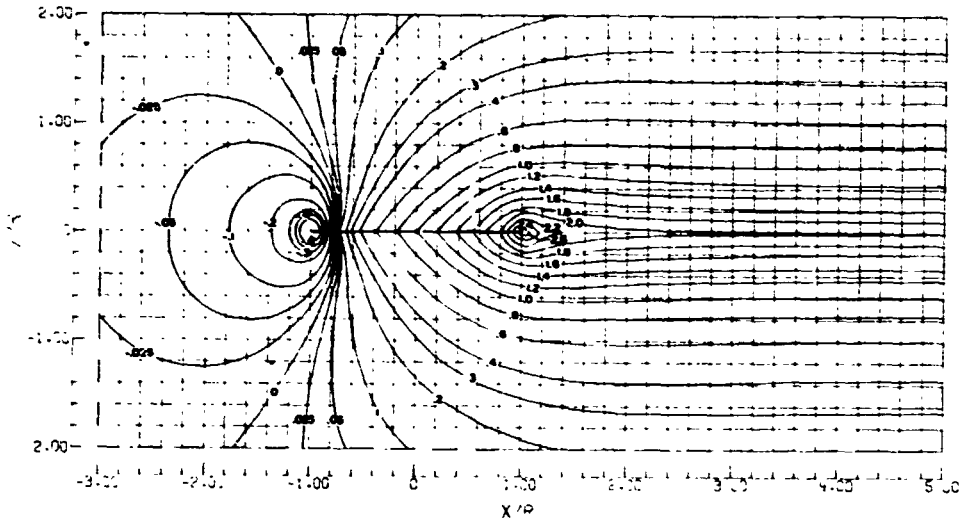

Contours of w/w_o

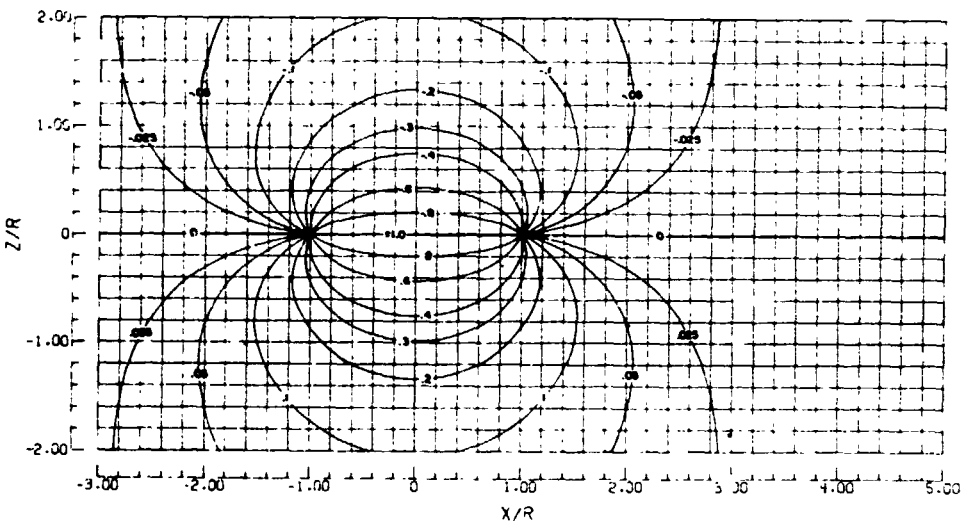

Contours of u/w_o
(j) $\chi = 90^o$

Figure 3. - Concluded.

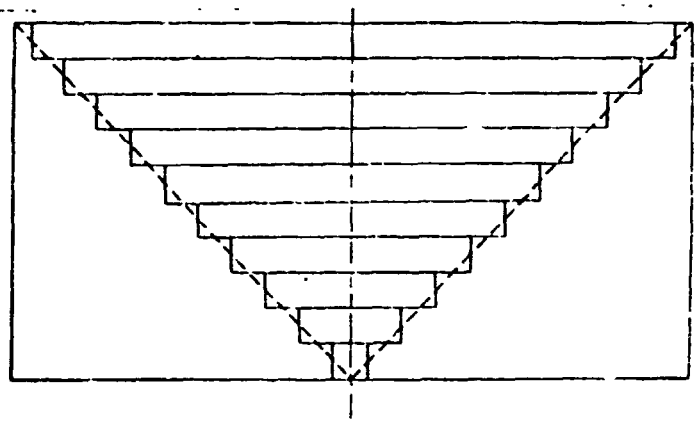

$\left(\frac{R_o}{R}\right)$	$\left(\frac{X}{R}\right)\left(\frac{R}{R_o}\right)$	$\left(\frac{Y}{R}\right)\left(\frac{R}{R_o}\right)$	$\left(\frac{Z}{R}\right)\left(\frac{R}{R_o}\right)$	$\left(\frac{v}{v_0}\right)_o$
1.00	0.200	0	0.100	1.15 (1.50) = 1.725
.95	.211	0	.106	1.15 (−.15) = −.173
.85	.236	0	.118	1.17 (−.15) = −.176
.75	.267	0	.131	1.19 (−.15) = −.179
.65	.308	0	.154	1.20 (−.15) = −.180
.55	.364	0	.182	1.21 (−.15) = −.182
.45	.445	0	.223	1.23 (−.15) = −.185
.35	.571	0	.286	1.24 (−.15) = −.186
.25	.800	0	.400	1.25 (−.15) = −.188
.15	1.330	0	.667	.95 (.15) = .143
.05	4.000	0	2.000	.26 (−.15) = −.039
				$r/r_0 = \Sigma(v/v_0)_o = 0.694$

Figure 4. - Triangular disk load distribution.

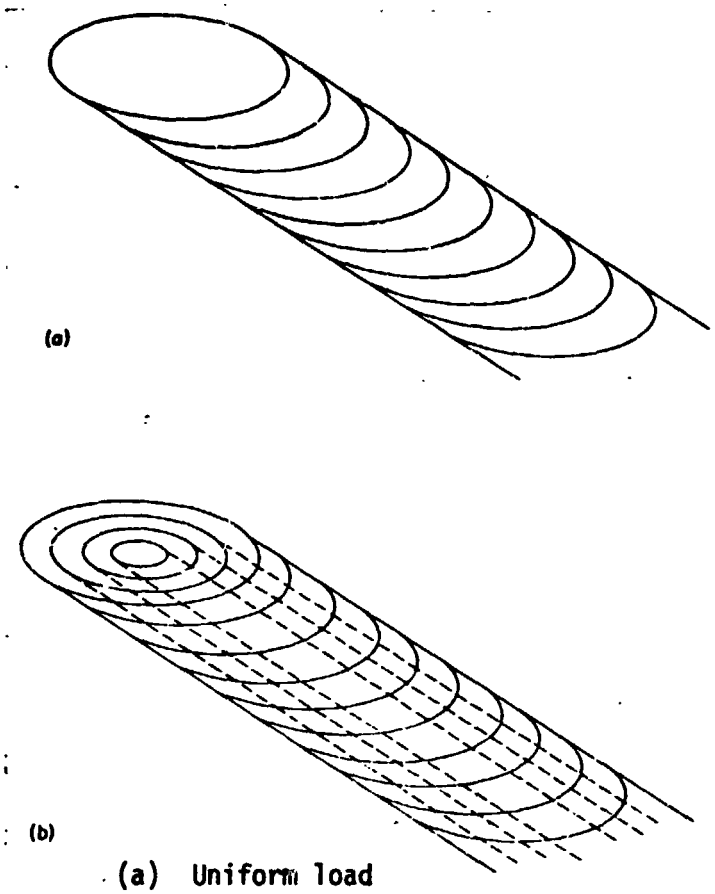

(a) Uniform load

(b) Nonuniform axially symmetric load.

Figure 5. - Assumed vortex pattern of rotor wake.

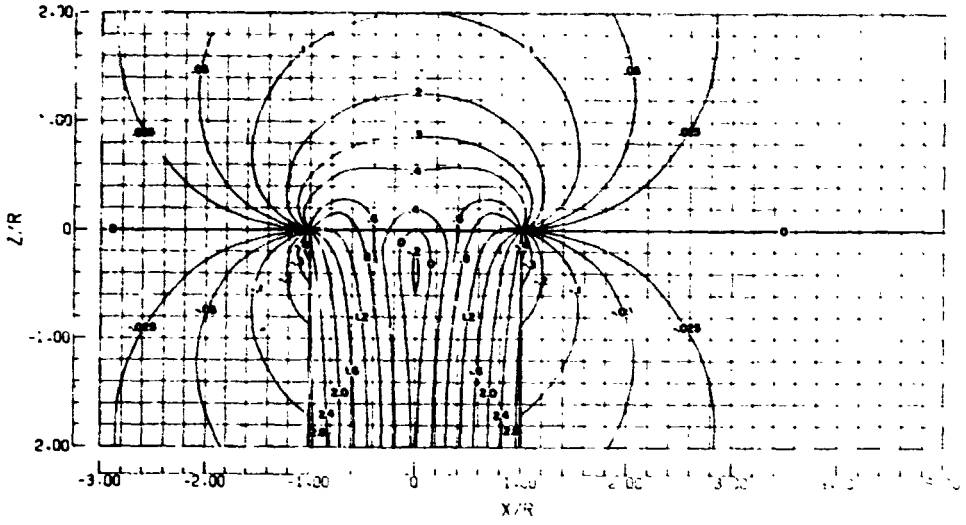

Contours of w/w_0

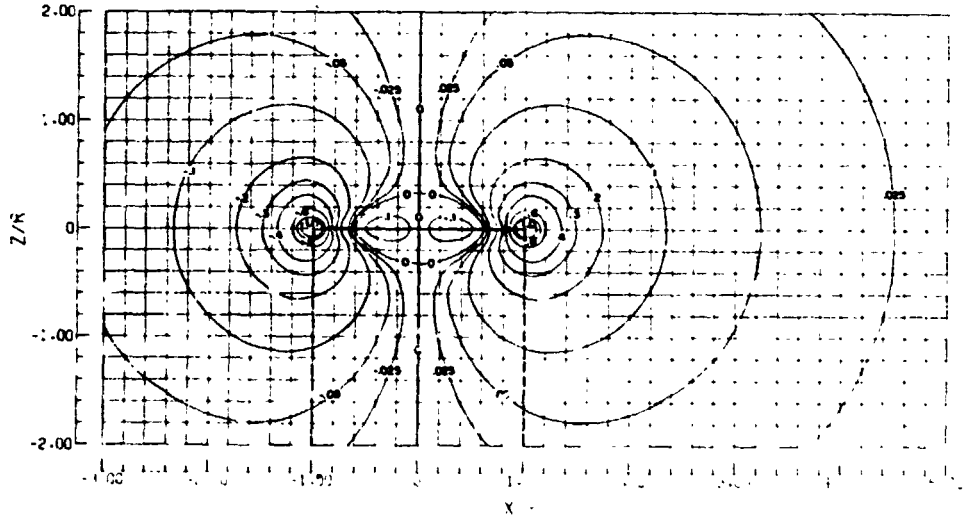

Contours of u/w_0
(a) χ - 0^0

Figure 6. - Induced velocities in the central longitudinal plane of a rotor with triangular disk load distribution.

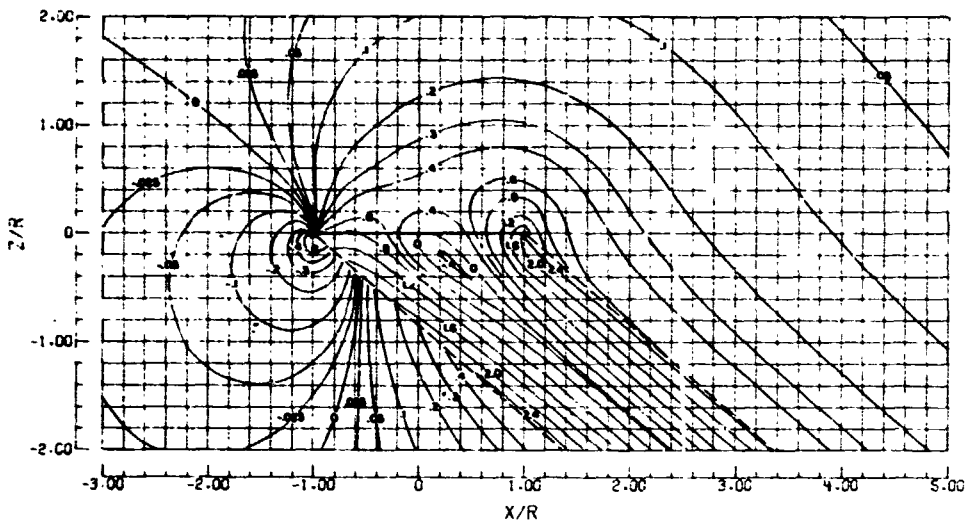

Contcurs of w/w_0

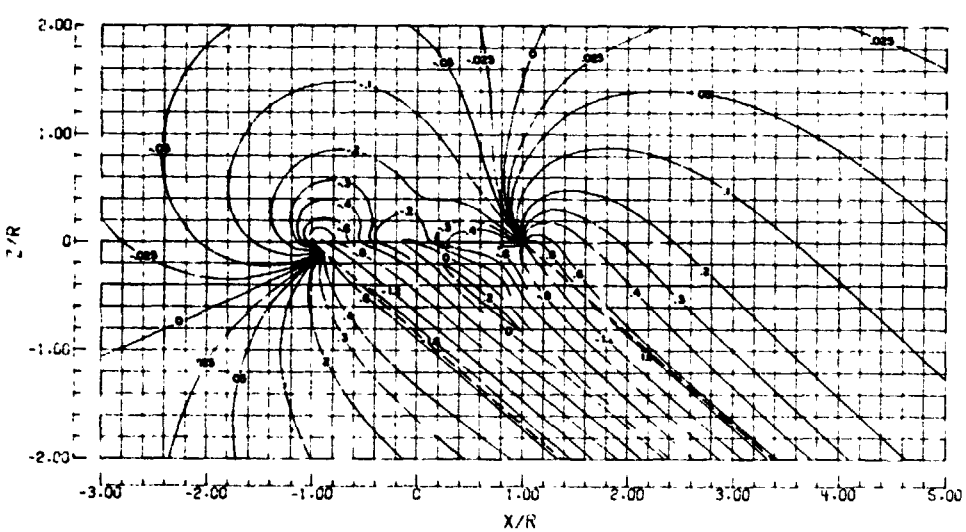

Contours of u/w^0
(b) $\chi = 50^0$
Figure 6. - Continued.

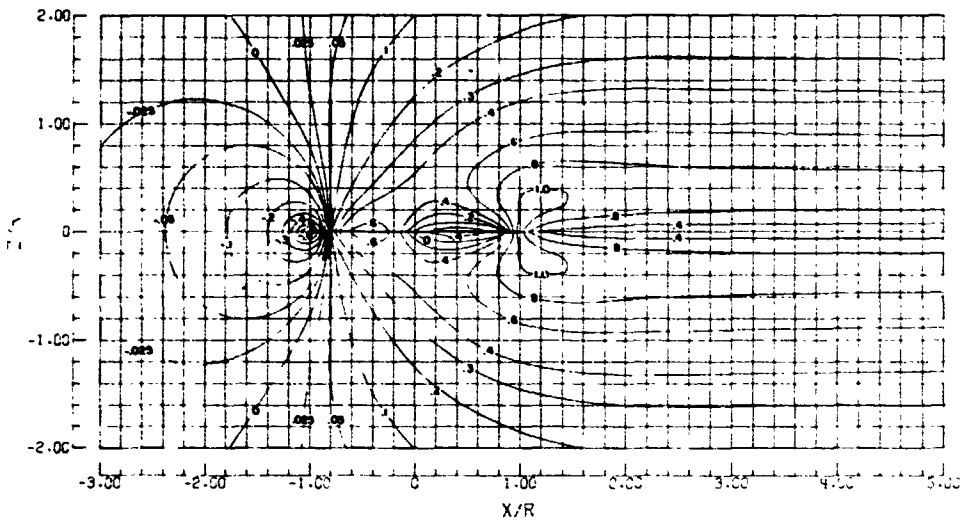

Contours of w/w_o

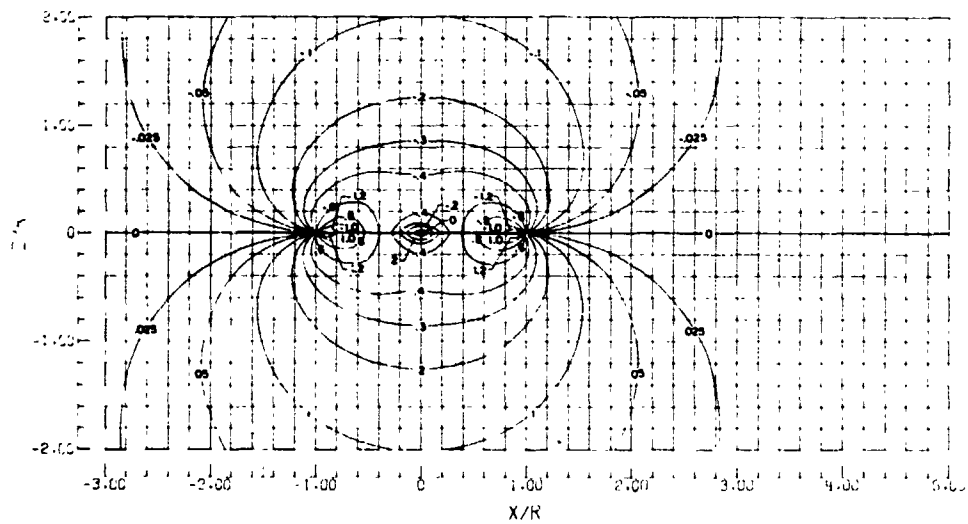

Contours of u/w_o
(c) $\chi = 90^o$
Figure 6. - Concluded.

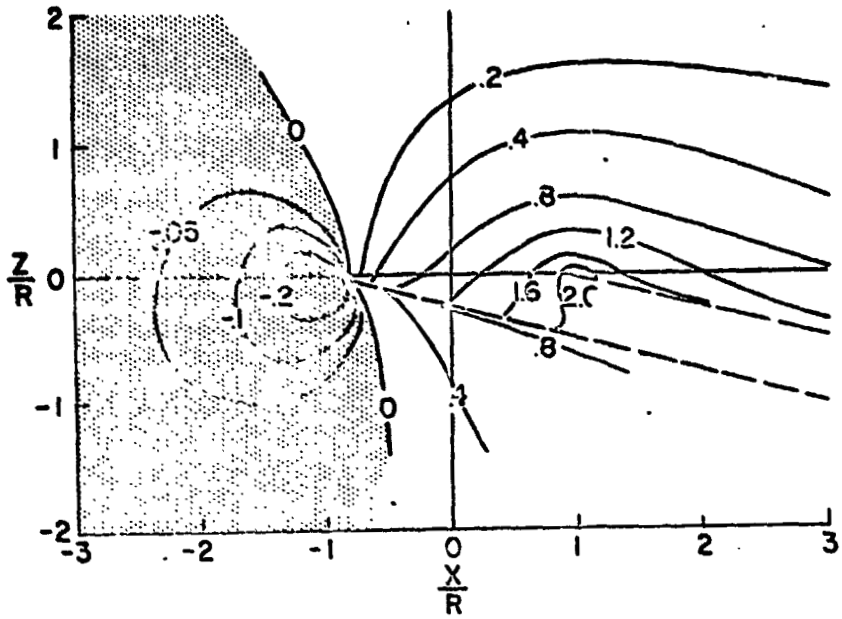

(a) Uniform disk loading

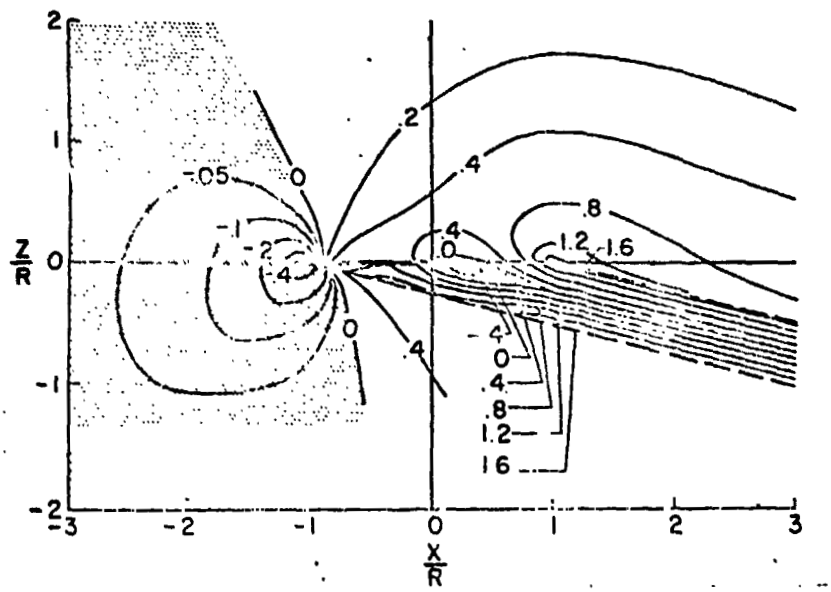

(b) Triangular disk loading

Figure 7. - Comparison of induced velocity ratios for uniform and triangular disk load distribution. $\chi = 76^{o}$.

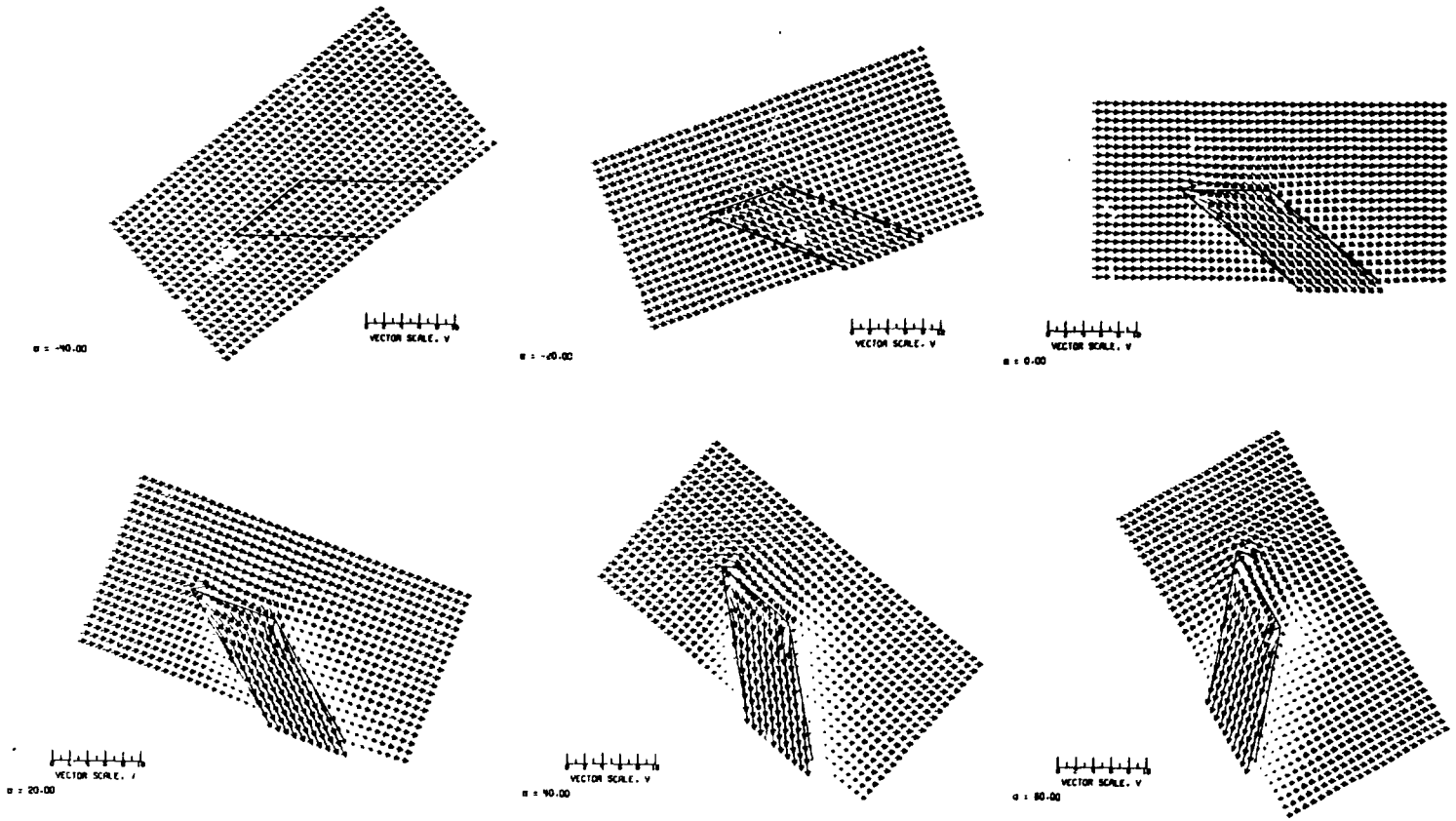

(a) Uniform disk loading.

Figure 8. - Flow field at different angles of attack with a single wake skew angle of 50°.

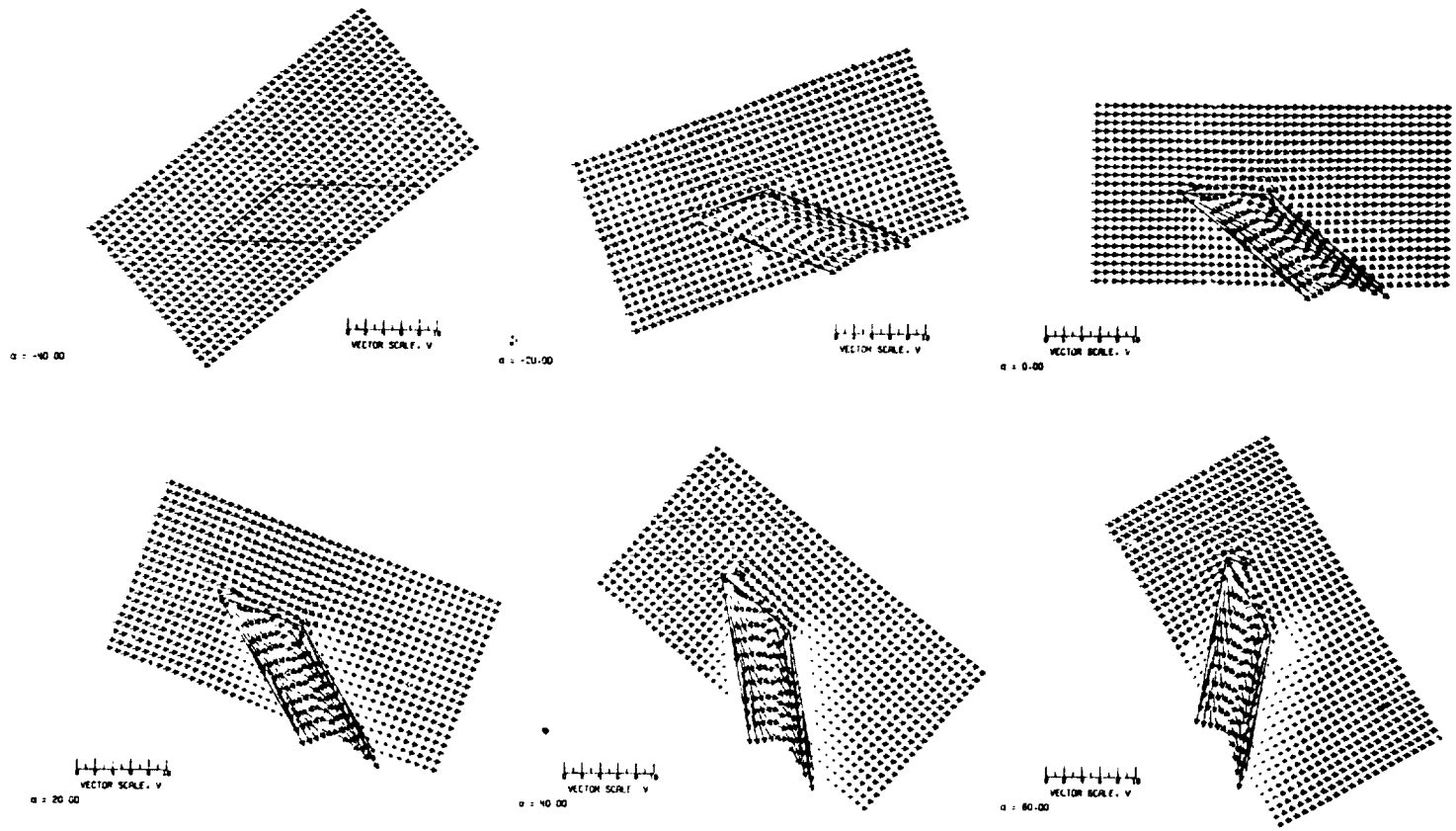

(b) triangular disk loading
Figure 8. - Concluded.

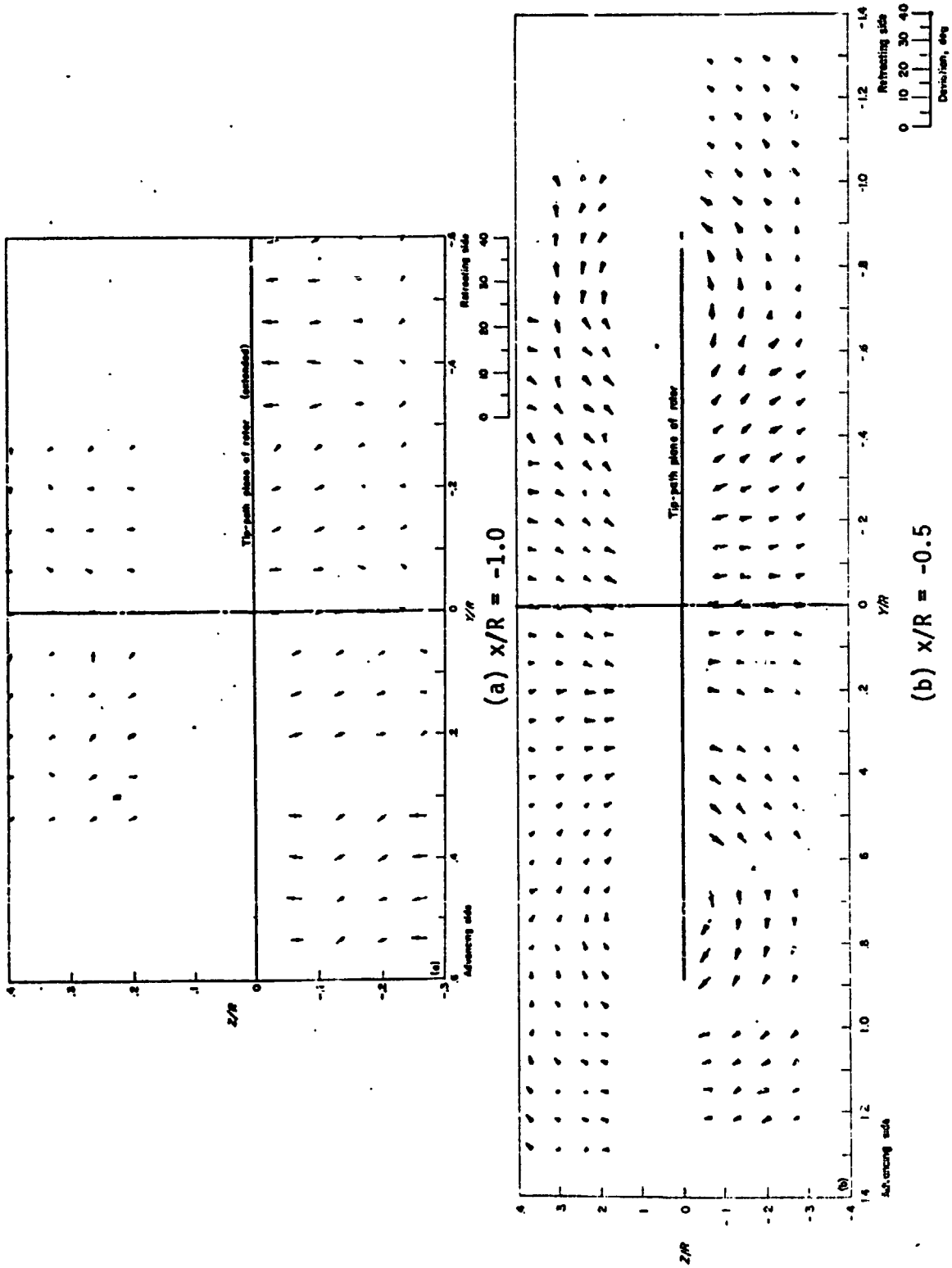

Figure 9. - Measured stream angles near a rotor. $\mu = 0.14$

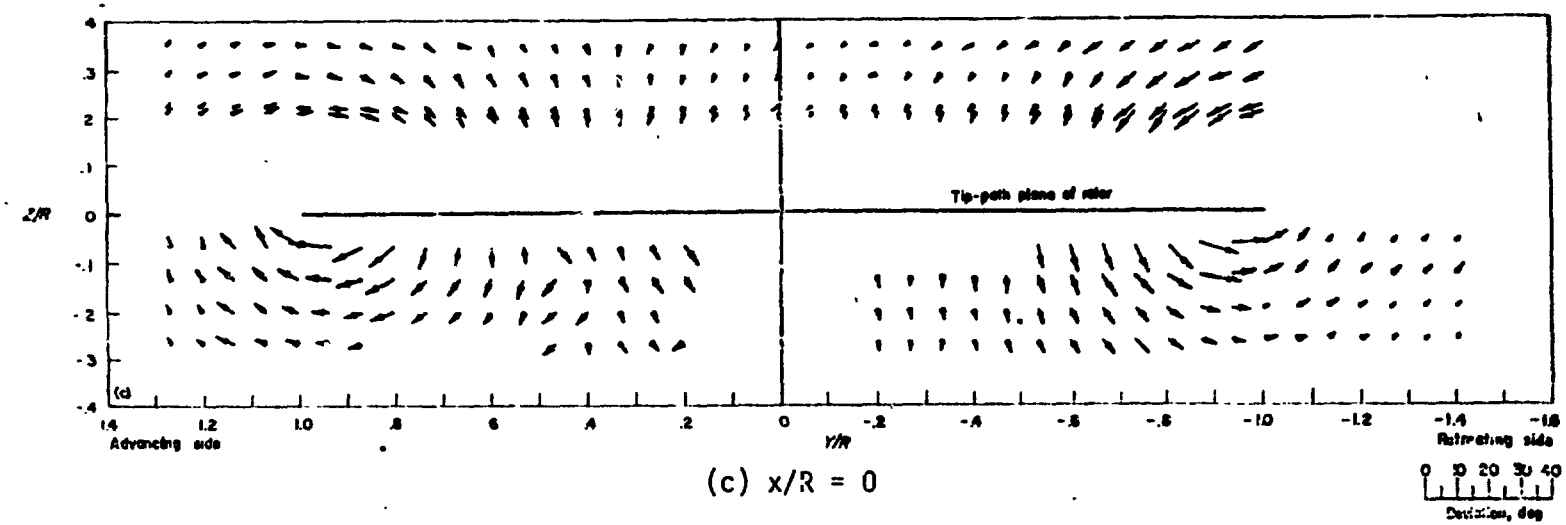

(c) x/R = 0

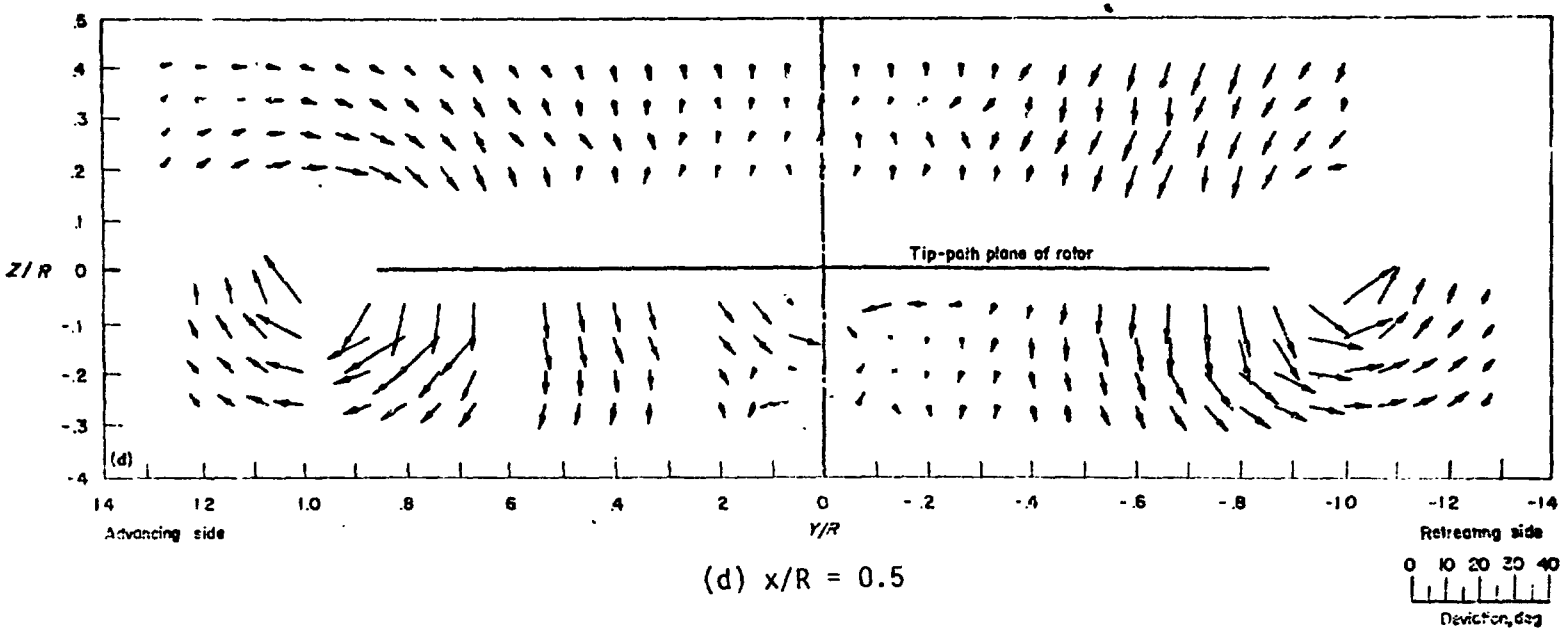

(d) x/R = 0.5

(c) $X/R = 0$.
(d) $X/R = 0.5$.

Figure 9. - Continued.

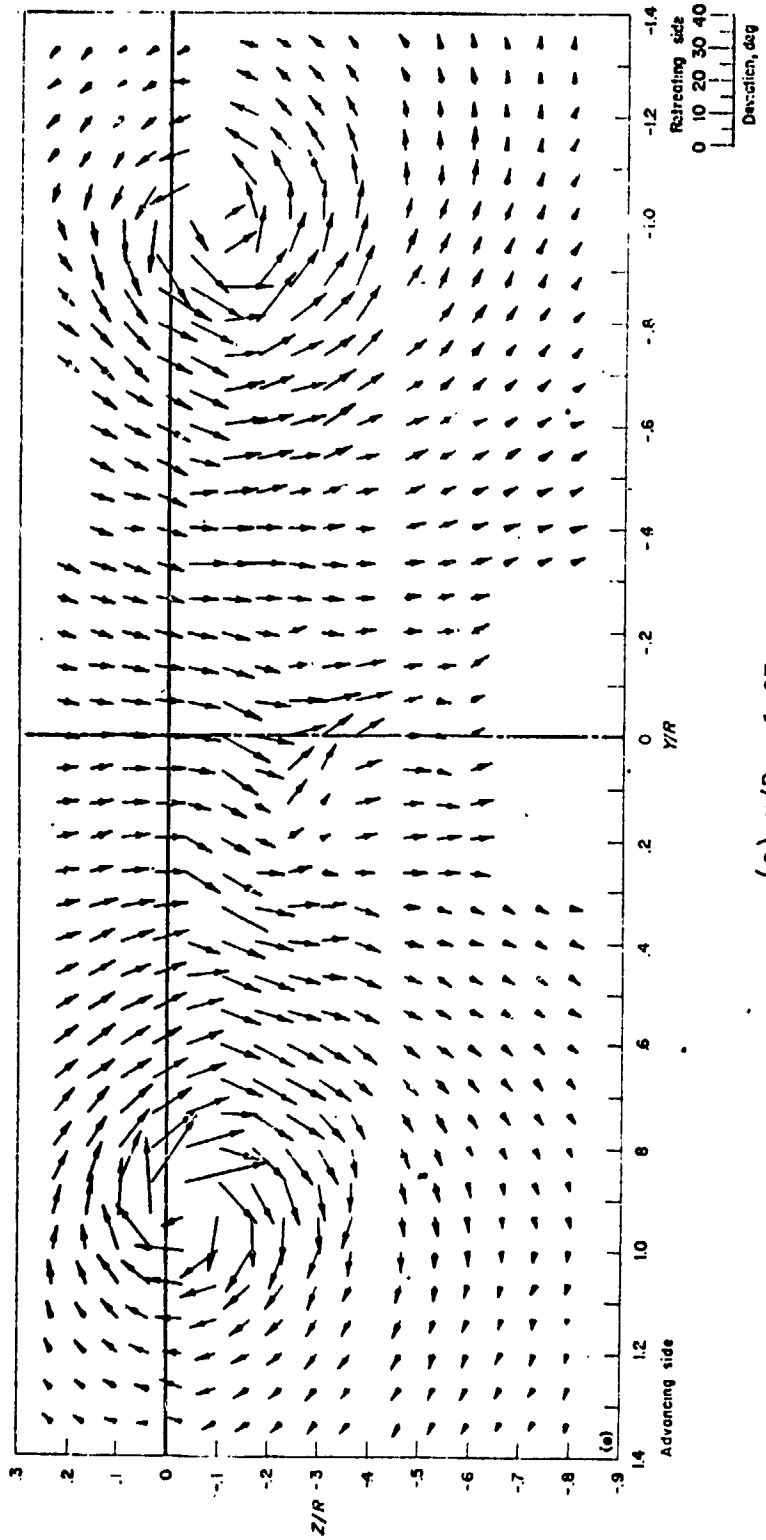

(e) $x/R = 1.07$

Figure 9. - Continued.

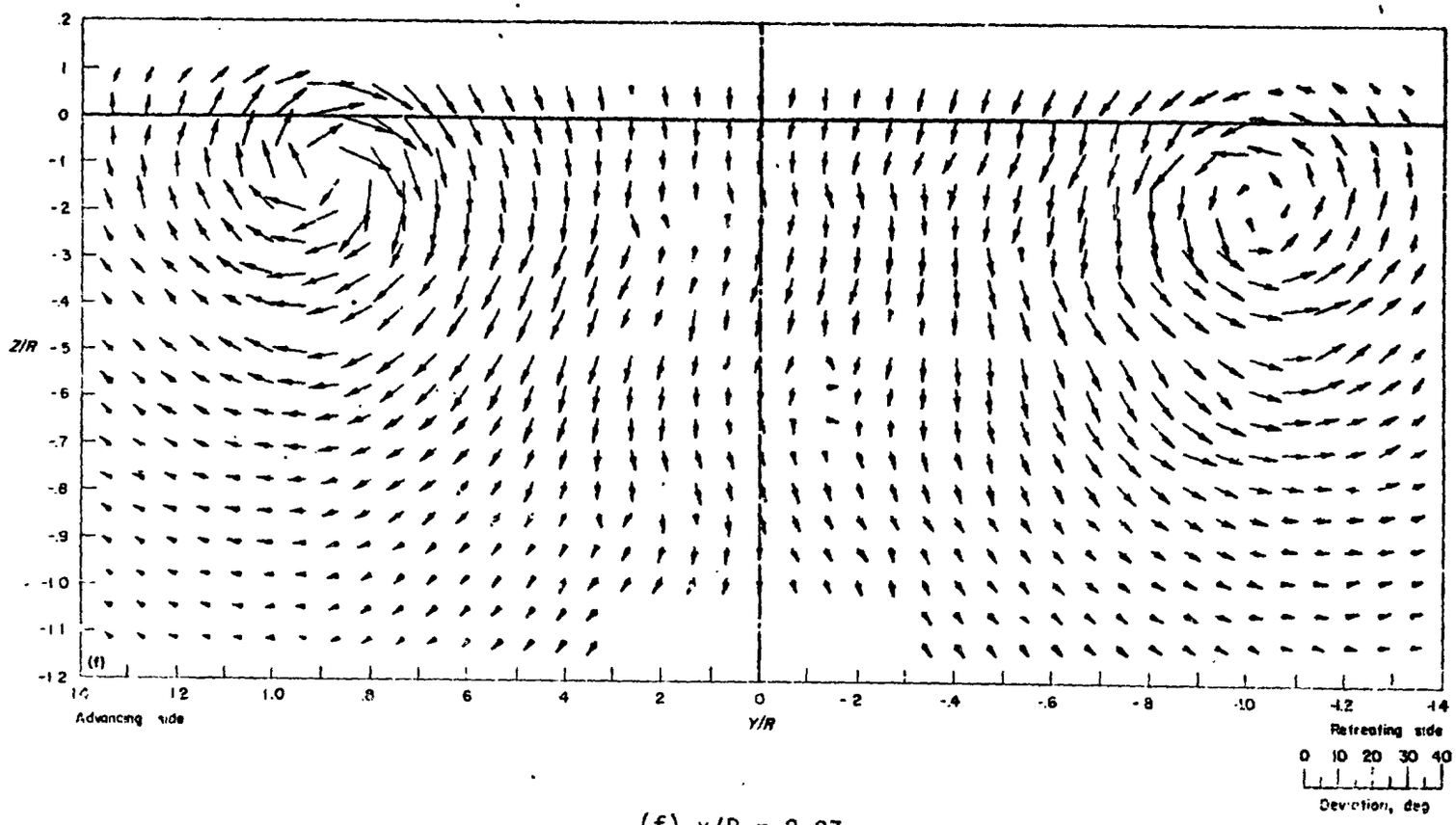

(f) x/R = 2.07

Figure 9. - Continued.

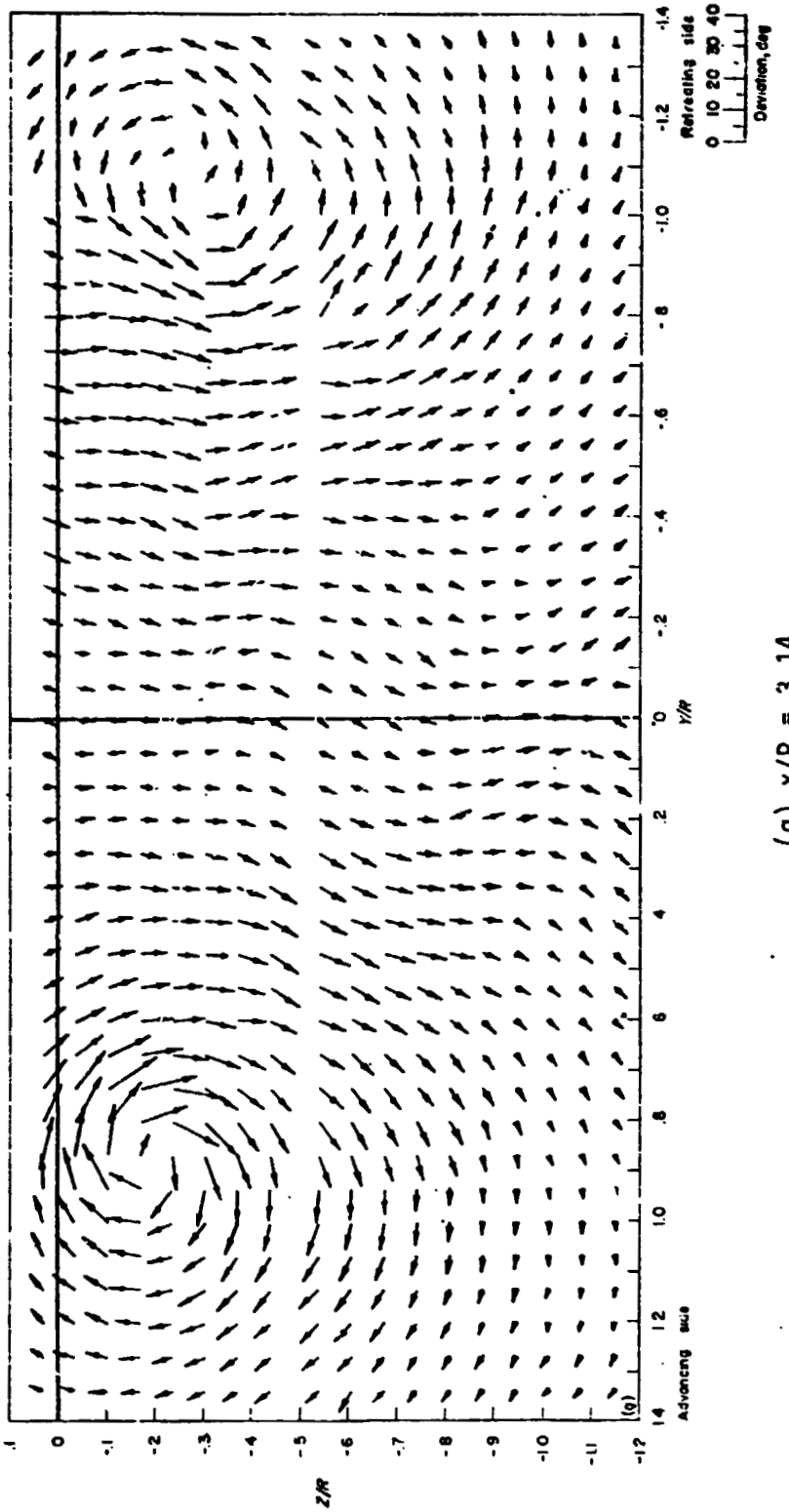

(g) x/R = 3.14

Figure 9. - Concluded.

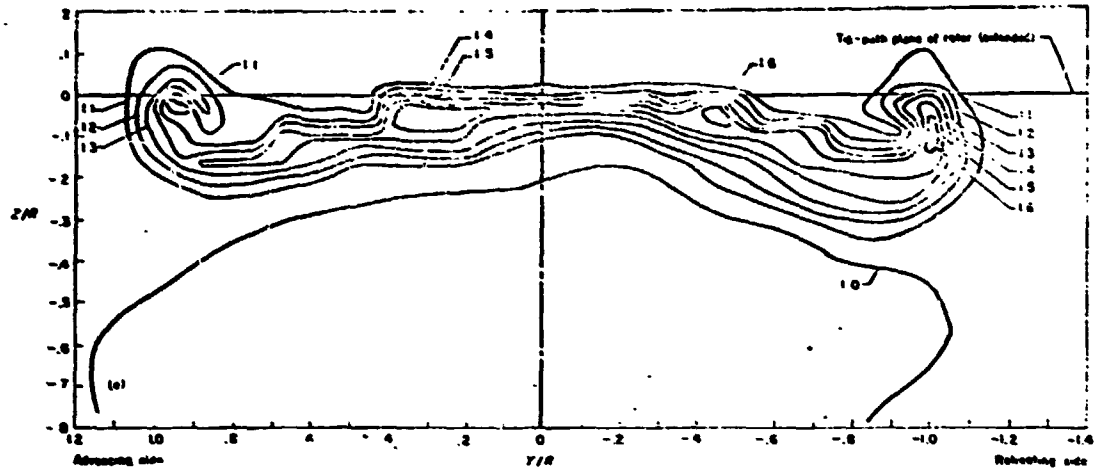

x/R = 1.07

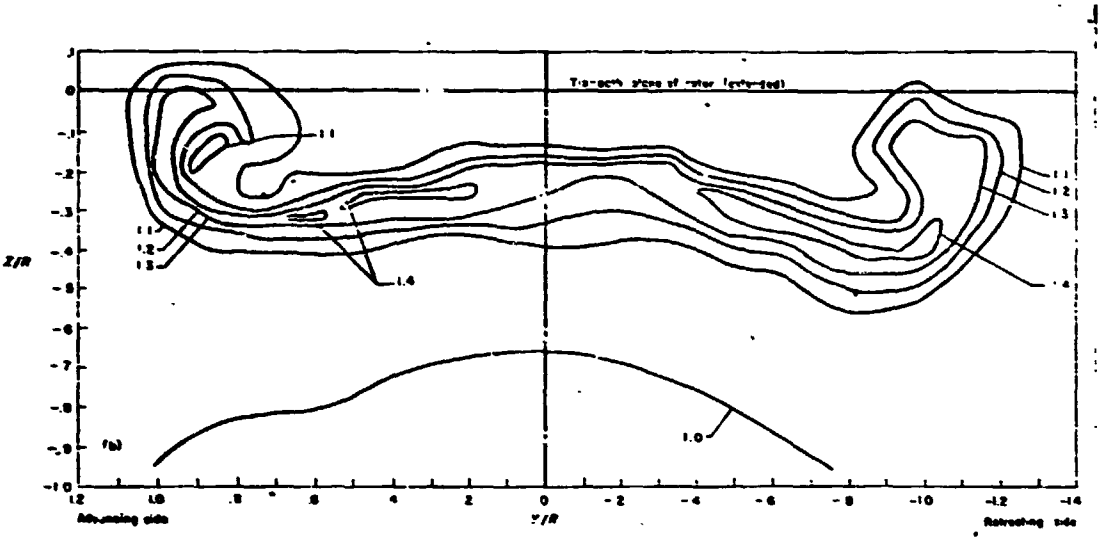

x/R = 2.07

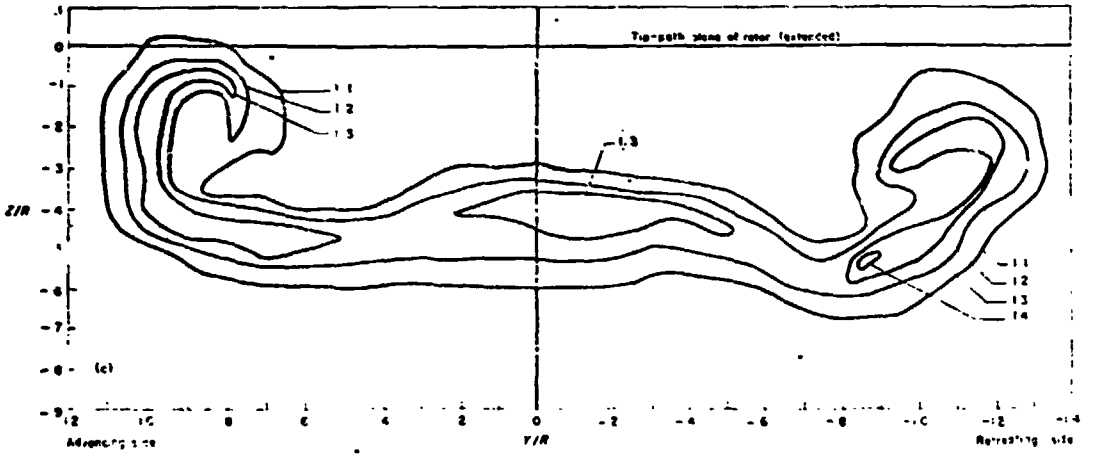

x/R = 3.14

Figure 10. - Contours of dynamic pressure behind a rotor. μ = 0.14.

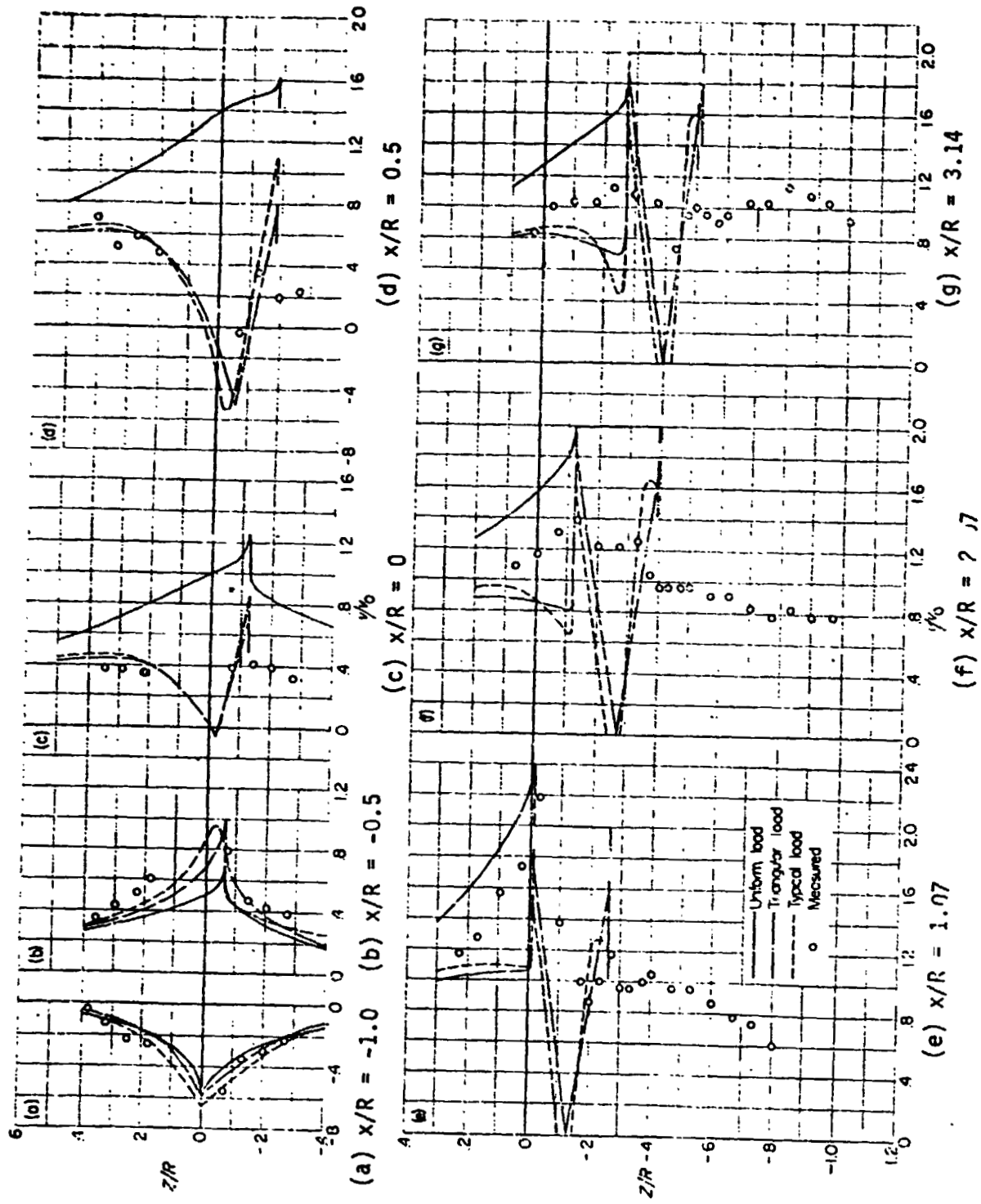

Figure 11. - Comparison of measured and theoretical values of induced-velocity ratio v/v_0 in longitudinal plane of symmetry. $\chi = 82.30$; $\mu = 0.140$

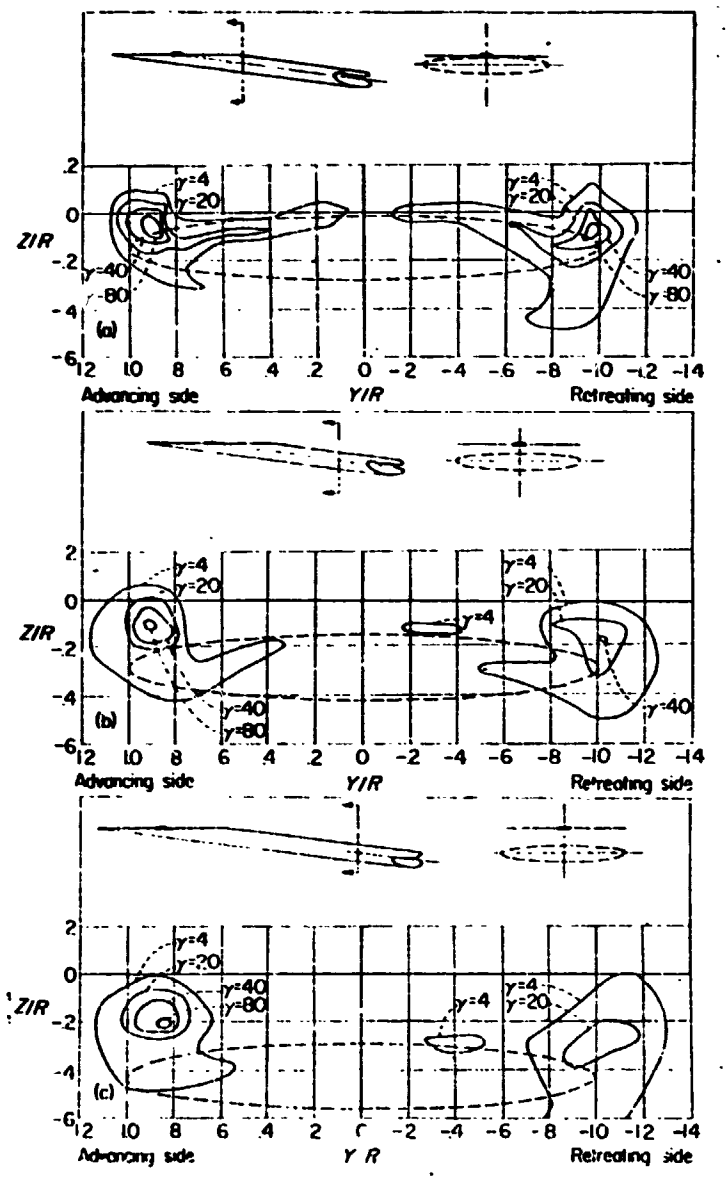

(a) x/R 1.07
(b) x/R = 2.07
(c) x/R = 3.14

Figure 12. - Distribution of vorticity behing rotor. χ = 32.3°; μ = 0.140

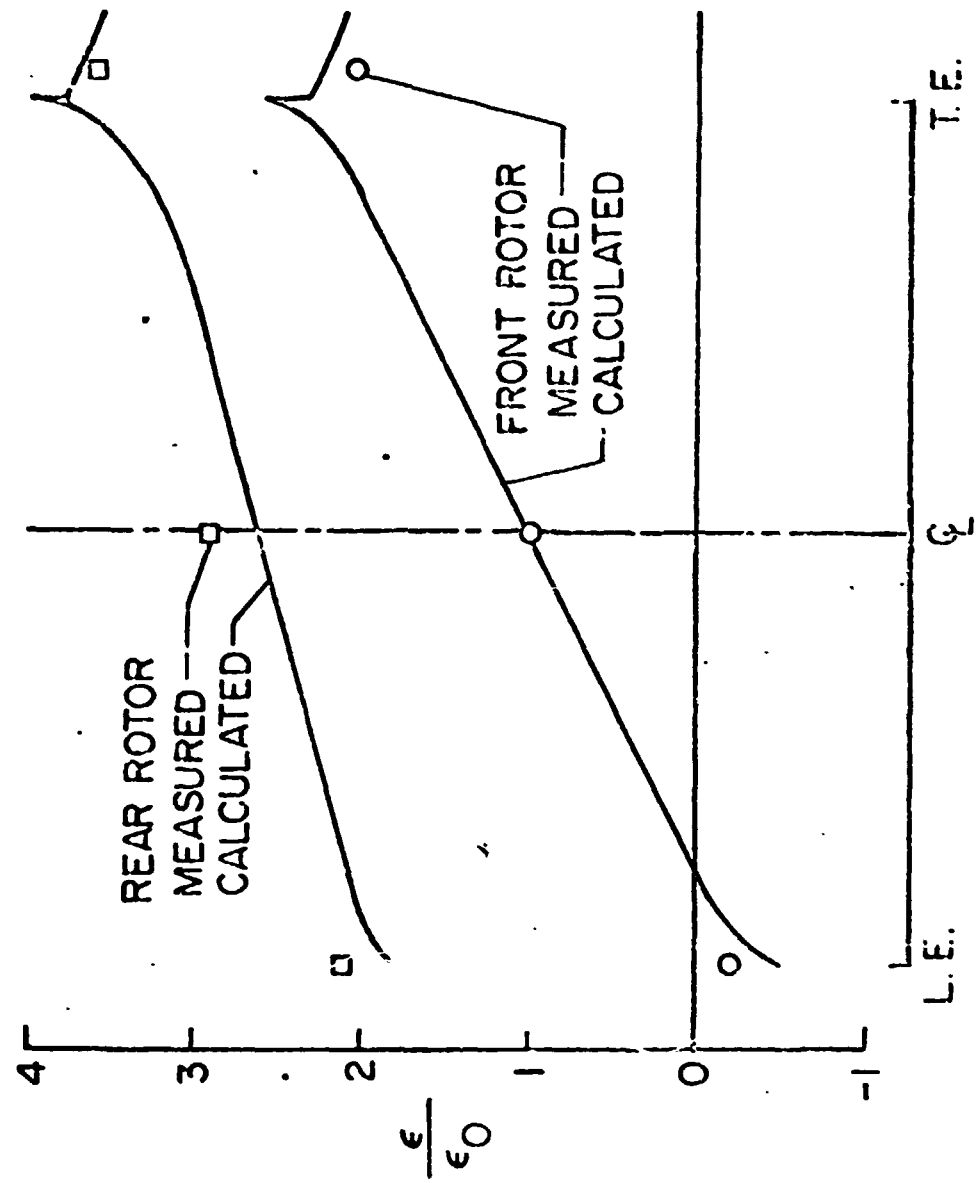

Figure 13. - Downwash of tandem rotors.

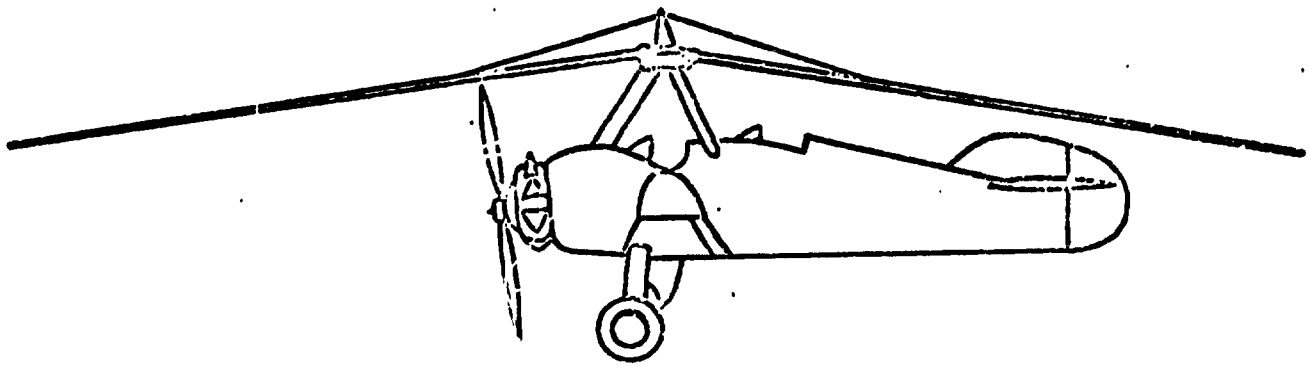

PCA-2 AUTOGYRO

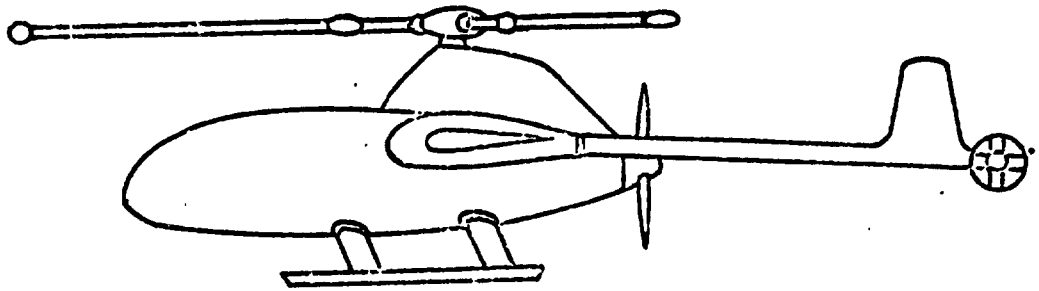

XV-1 CONVERTIPLANE

Figure 14. - Two unloaded rotor aircraft

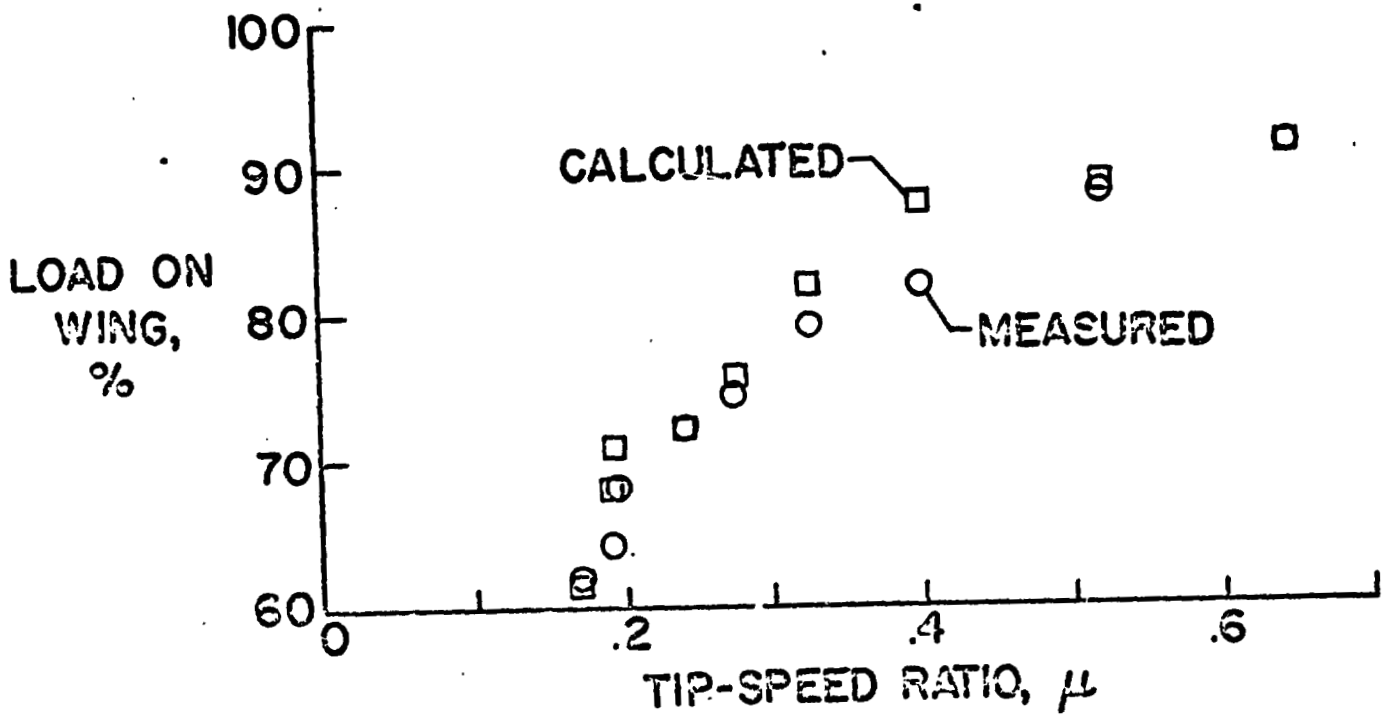

Figure 15. - Division of load between wing and rotor of PCA-2 autogyro.

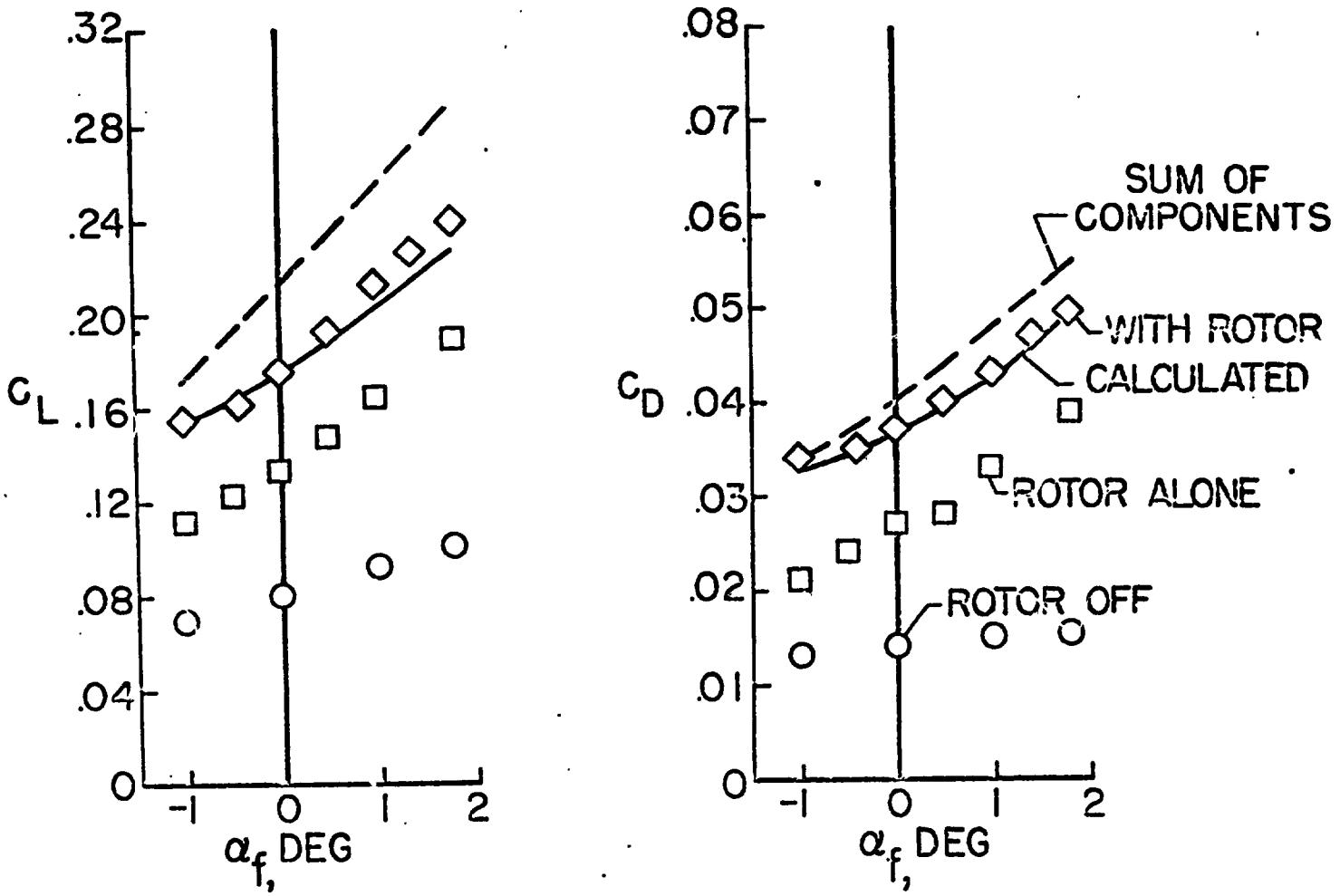

(a) Lift coefficient

(b) drag coefficient

Figure 16. - Performance of XV-1 at 100 knots.

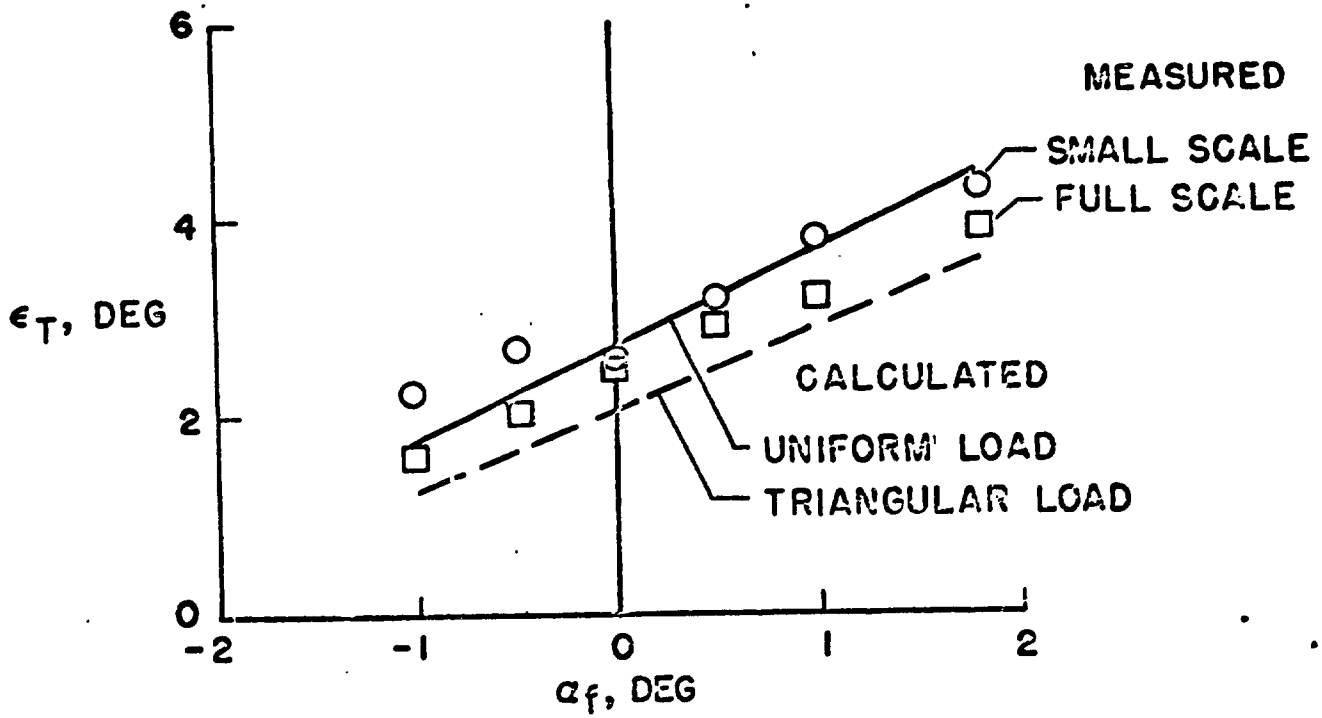

Figure 17. - Downwash at tail of XV-1 at 100 knots.

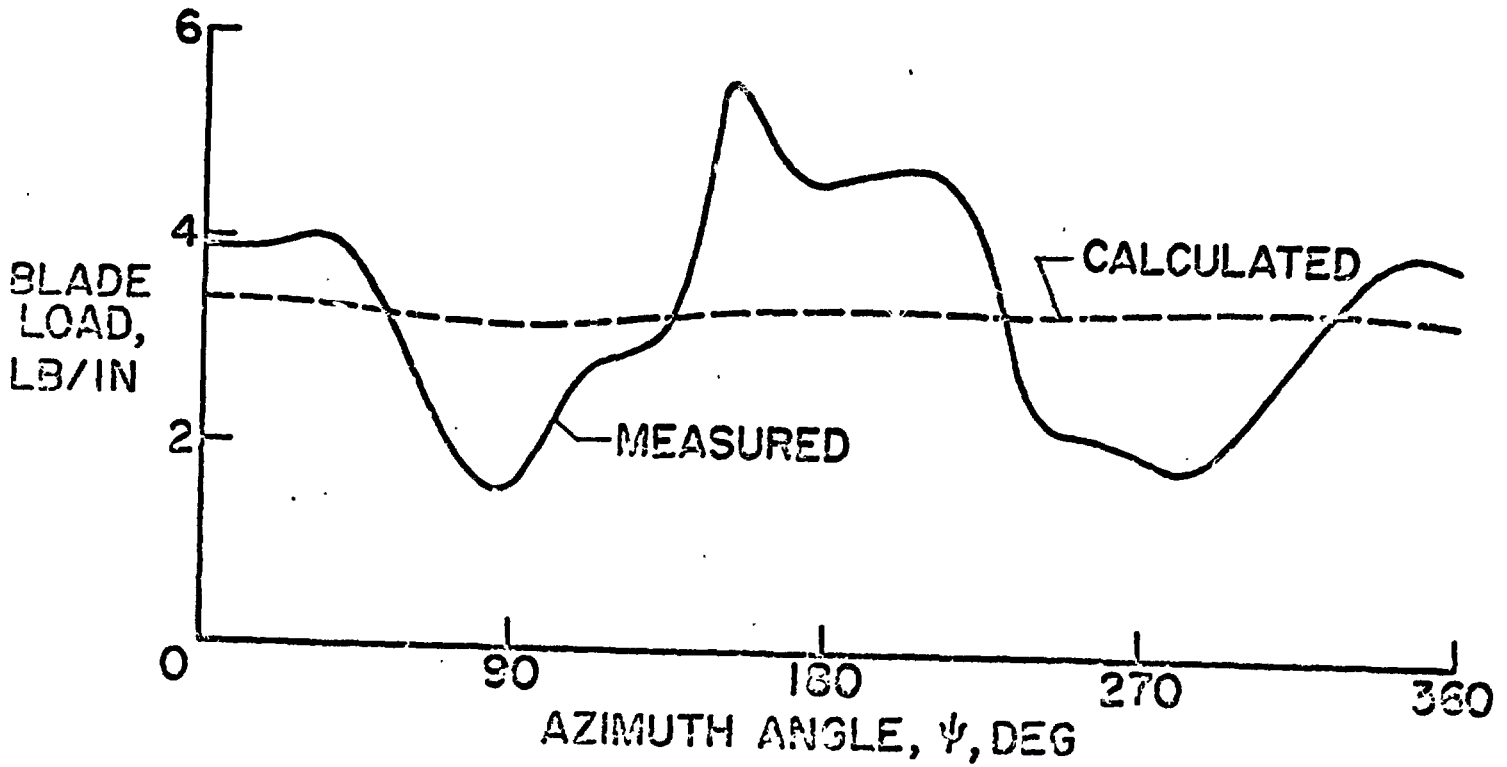

Figure 18. - Blade load at three-quarter radius as obtained from blade pressure distribution measurements. $\mu = 0.08$.

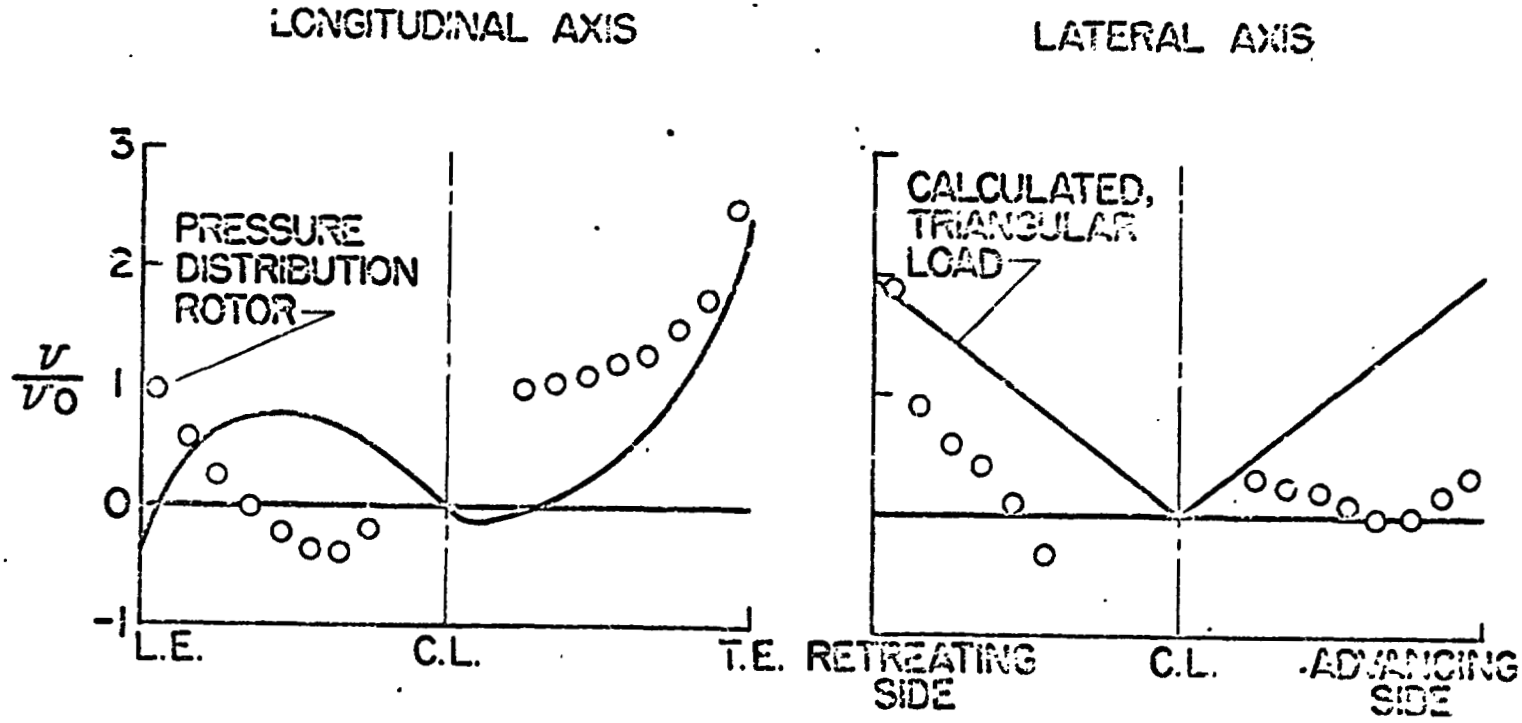

(a) Longitudinal axis

(b) Lateral axis

Figure 19. - Comparison of calculated time-average induced velocity in the plane of the rotor with the effective induced velocity as determined from pressure-distribution measurements on a rotor blade. $\mu = 0.30$.

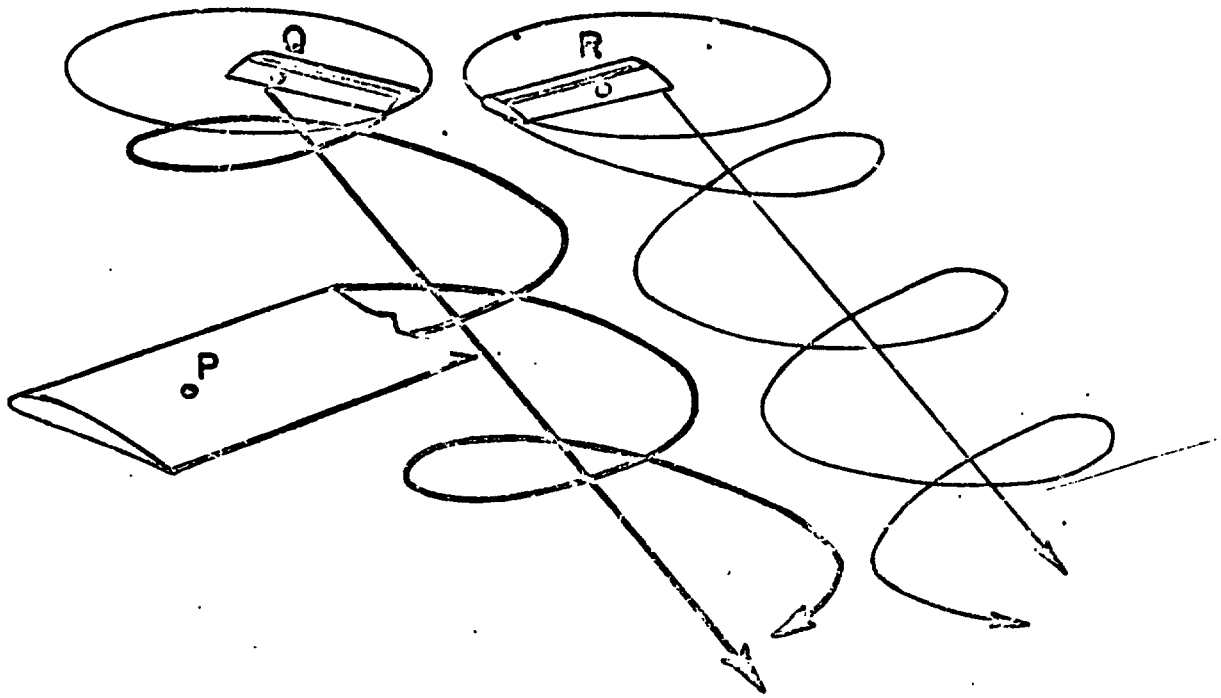

Figure 20. - Effect of theoretical assumptions on use of calculated induced velocities.

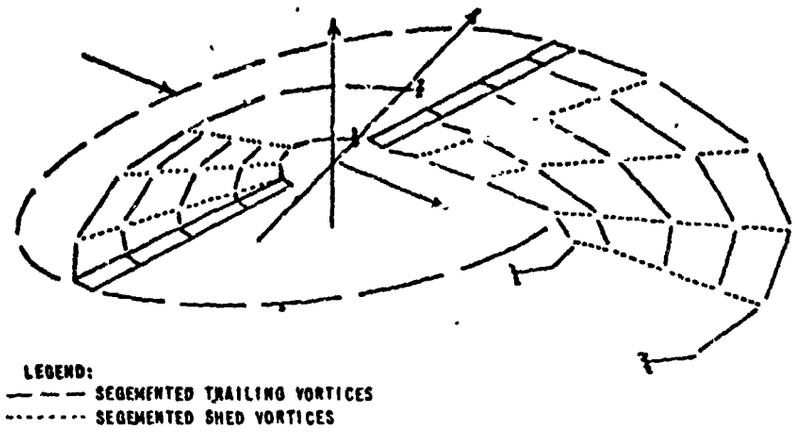

Figure 21. - Vortex wake used by Piziali and Duwaldt in reference 17.

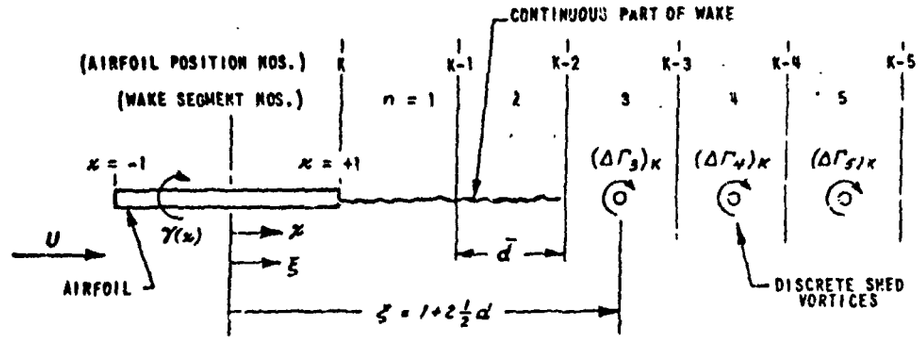

Figure 22. - Blade representation used in reference 18 by Daughaday and Piziali.

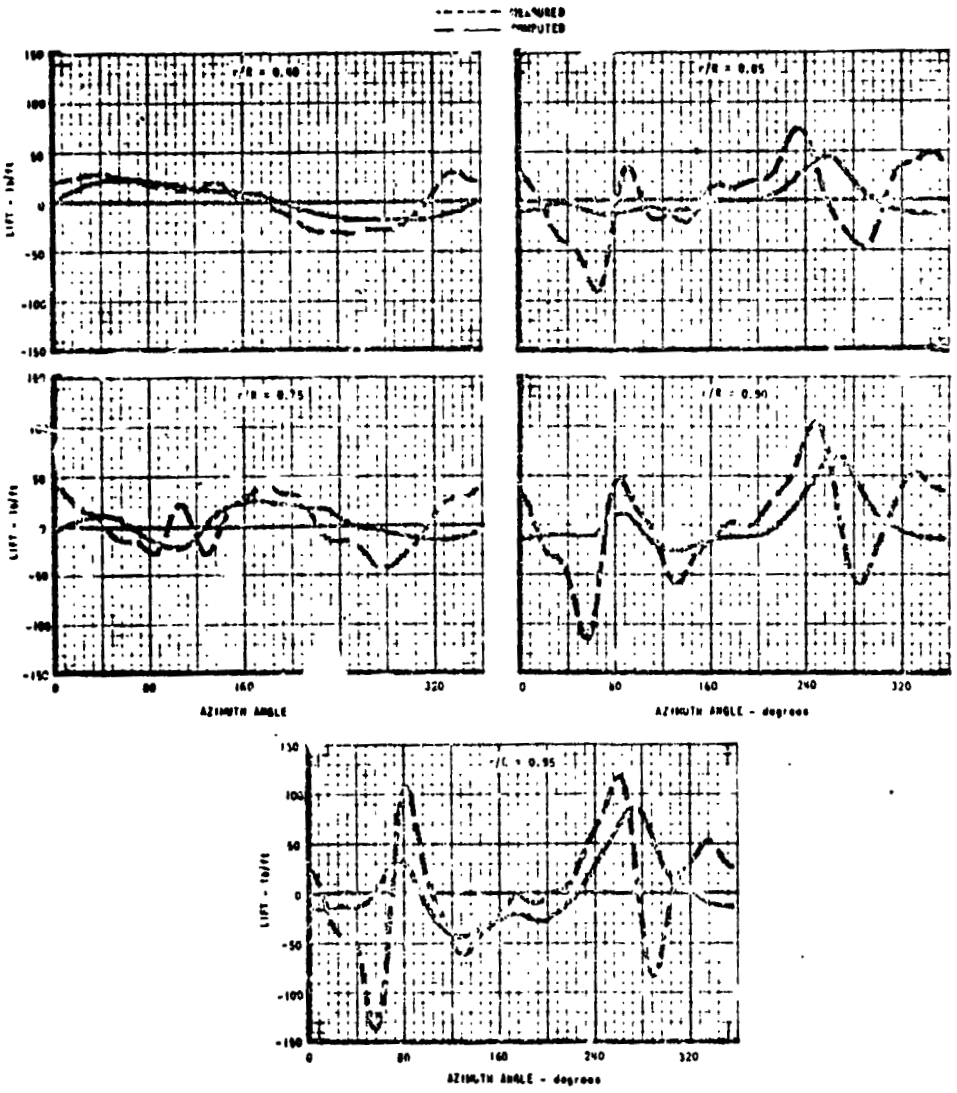

Figure 23. - Measured and computed lifts from Piziali's analysis. HU-1A at $\mu = 0.08$.

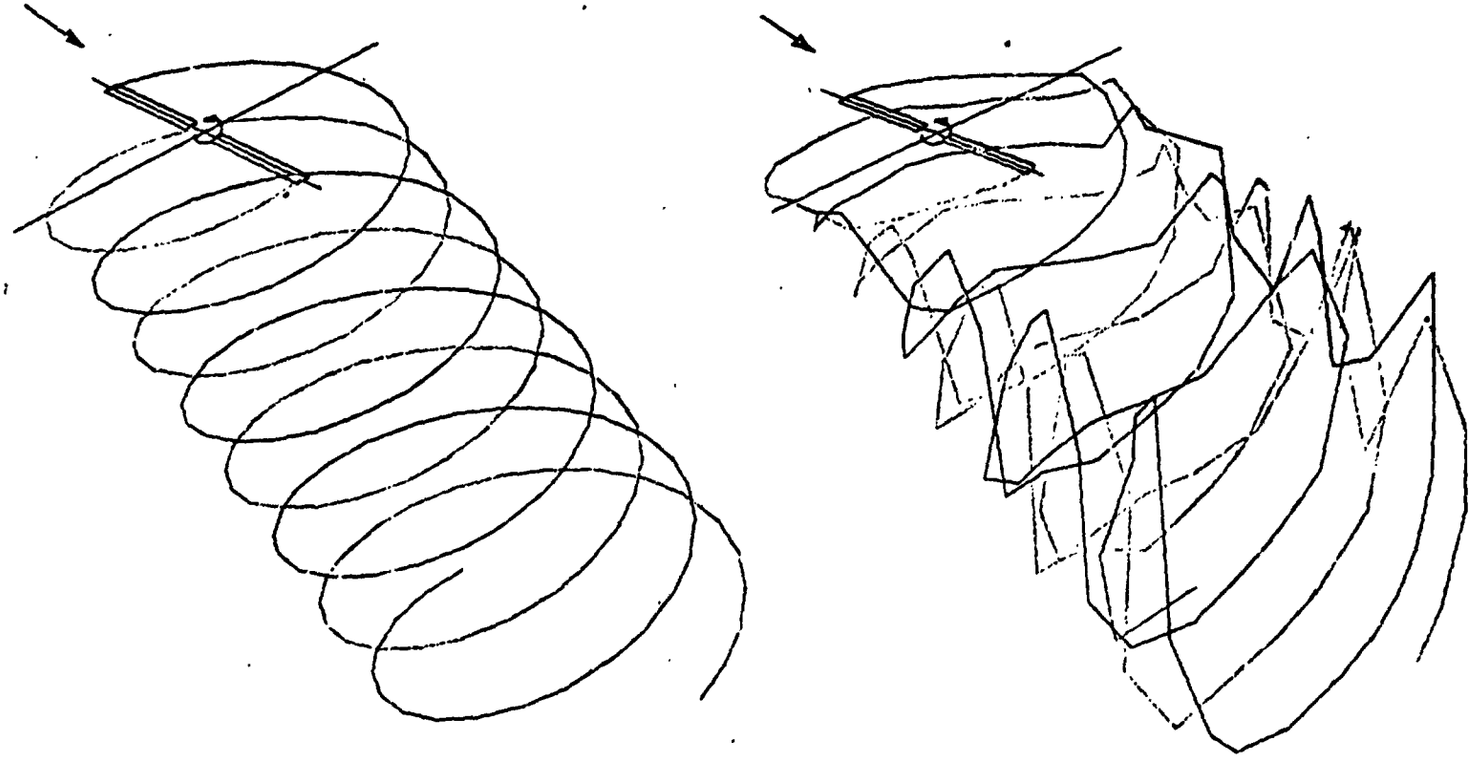

Skewed Helical Wake Configuration

Distorted Wake

Figure 24. - Crimi's calculation of wake distortions

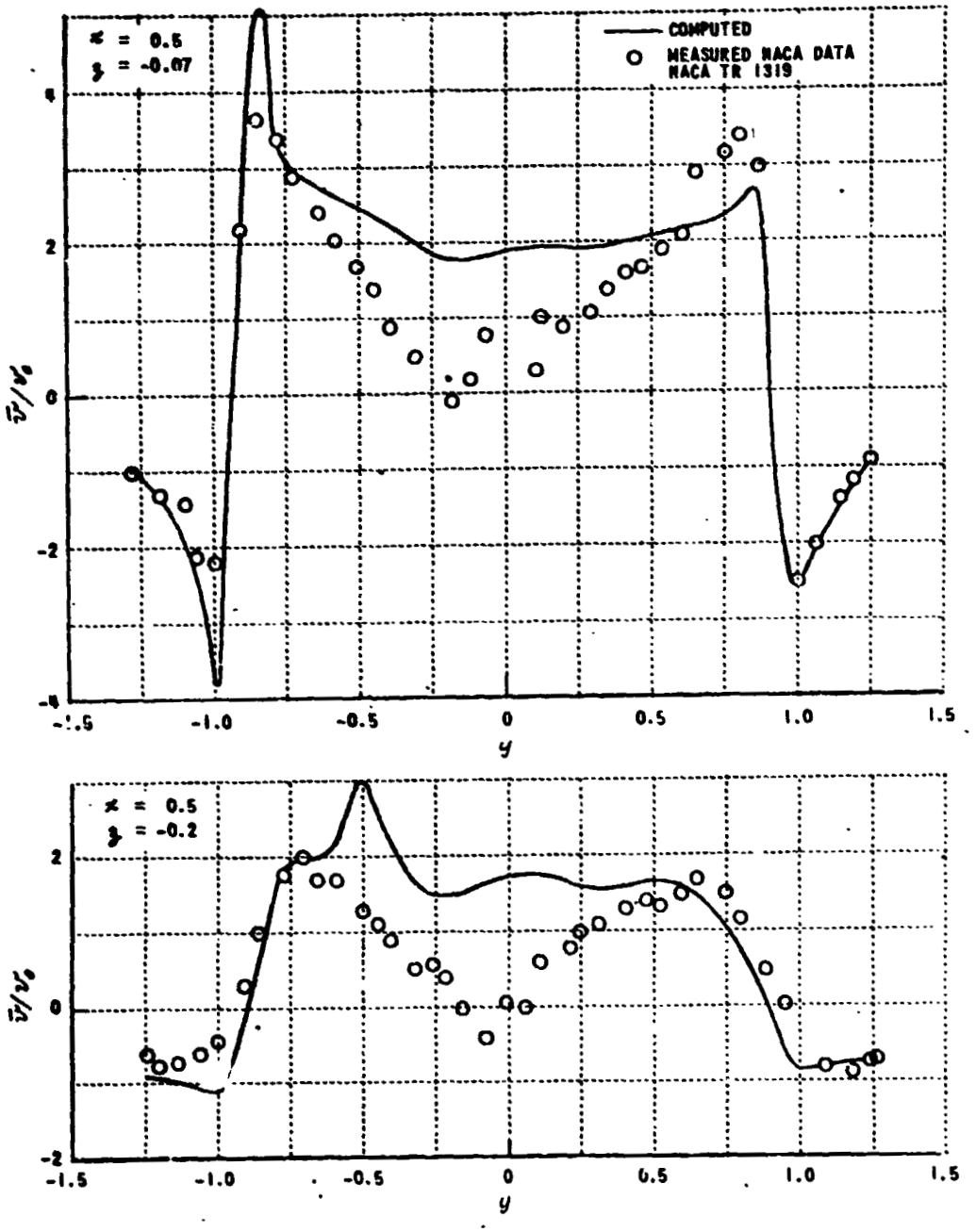

Figure 25. - Comparison of computed and measured induced downwash below the rotor plane, $\mu = 0.14$, $C = 0.00371$, $\chi = 0.5$.

ORIGINAL PAGE IS
OF POOR QUALITY

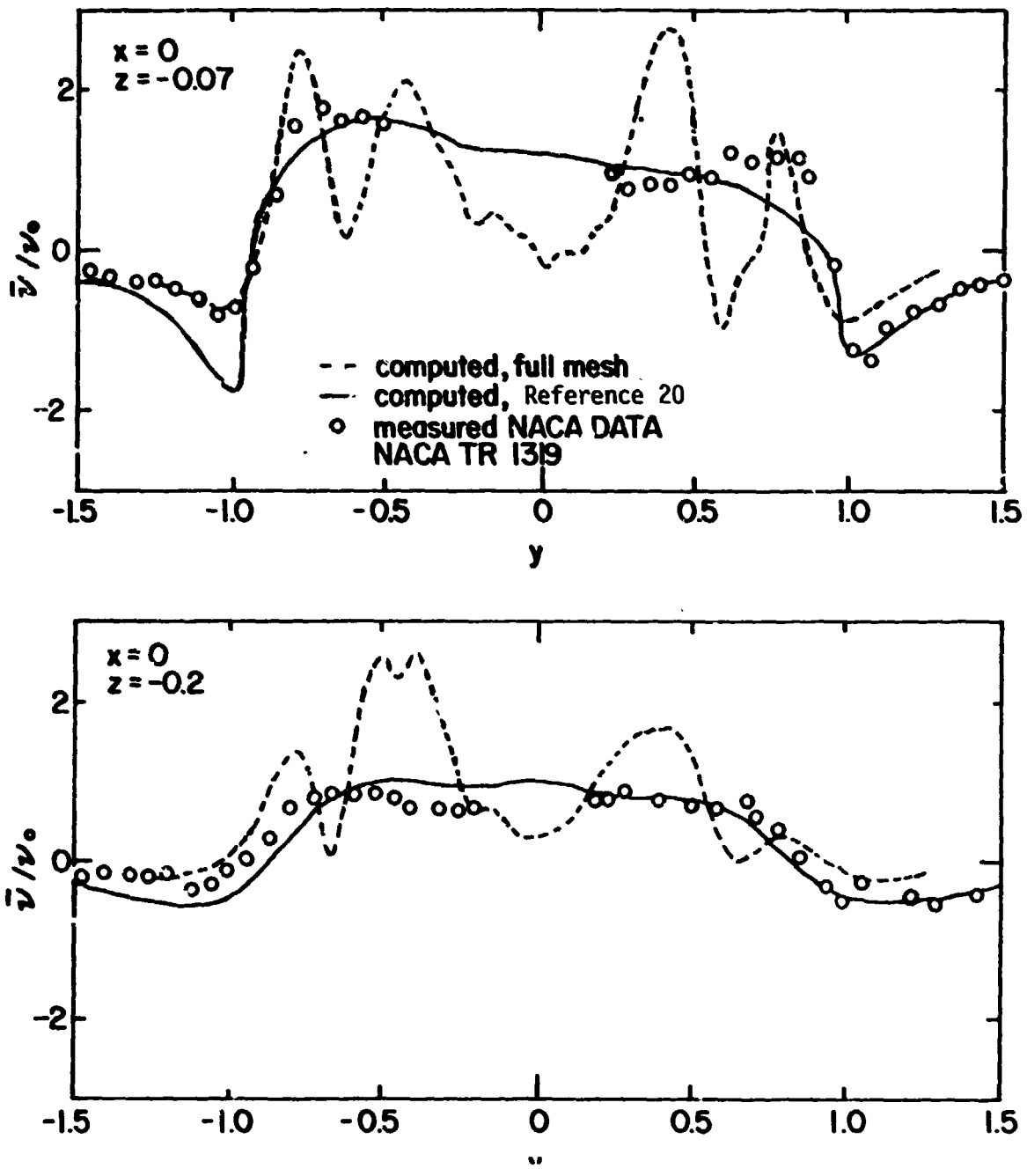

Figure 26. - Comparison of computed and measured induced below the rotor plane, $\mu = 0.14$, $C = 0.00371$, $x = 0$.

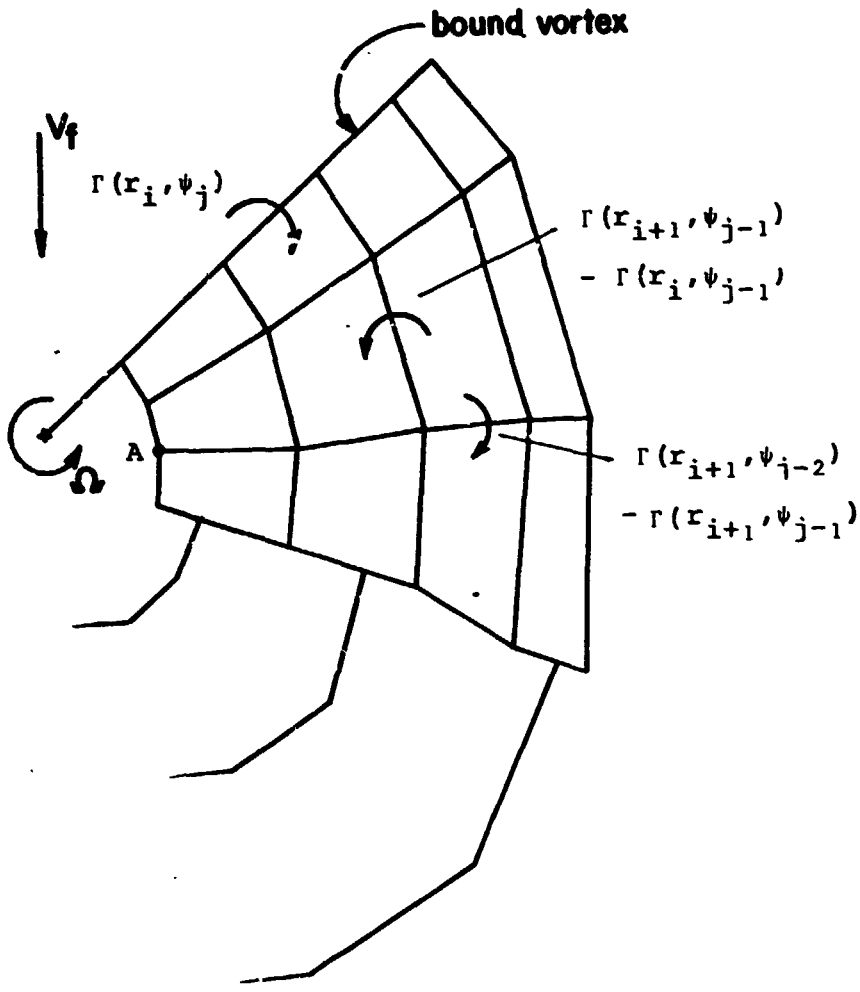

Figure 27. - Wake model with combination of "full mesh" wake and "modified" wake of trailing vortices only.

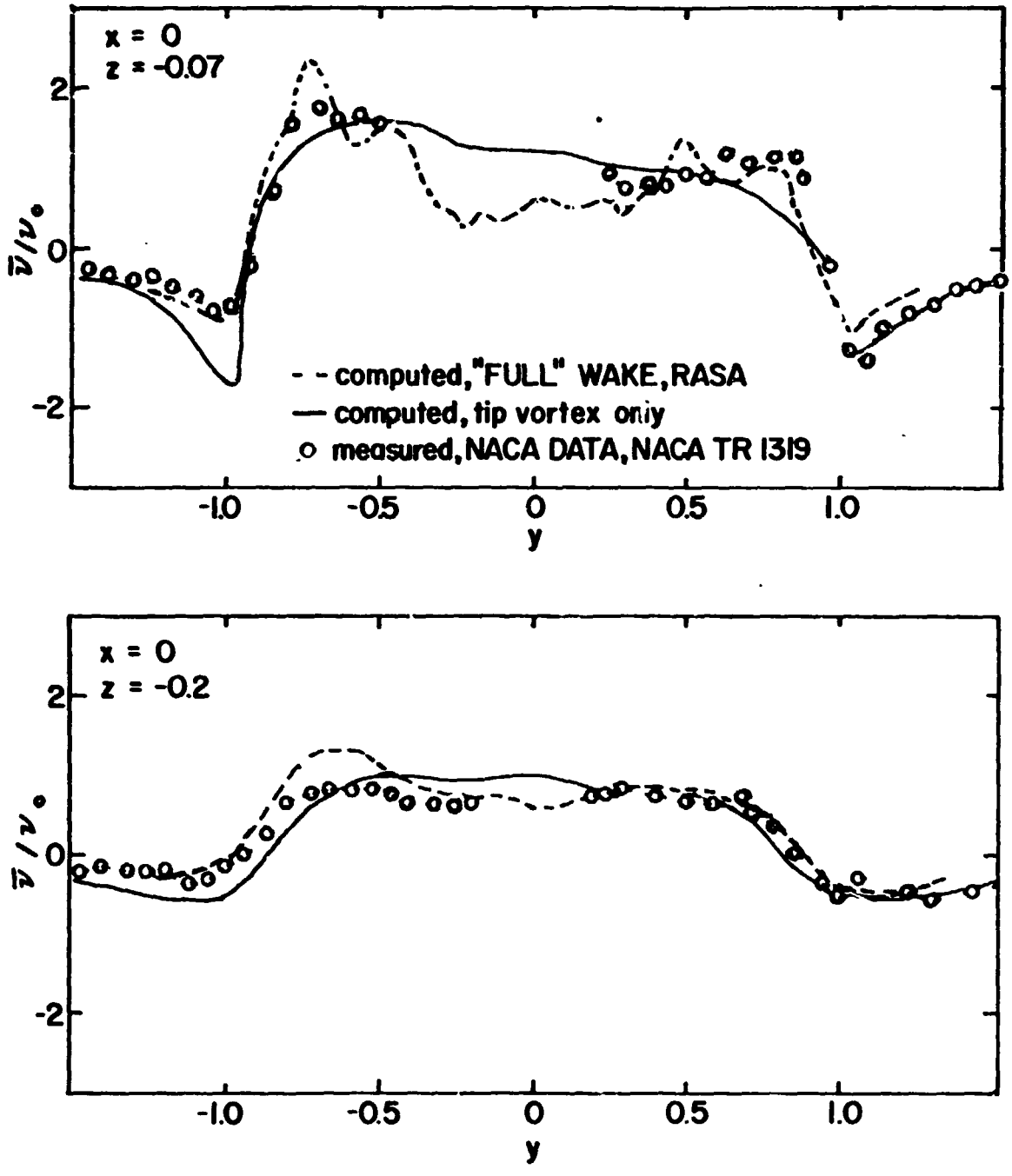

Figure 28. - Comparison of computed and measured induced below the rotor plane, $\mu = 0.14$, $C = 0.00371$, $x = 0$.

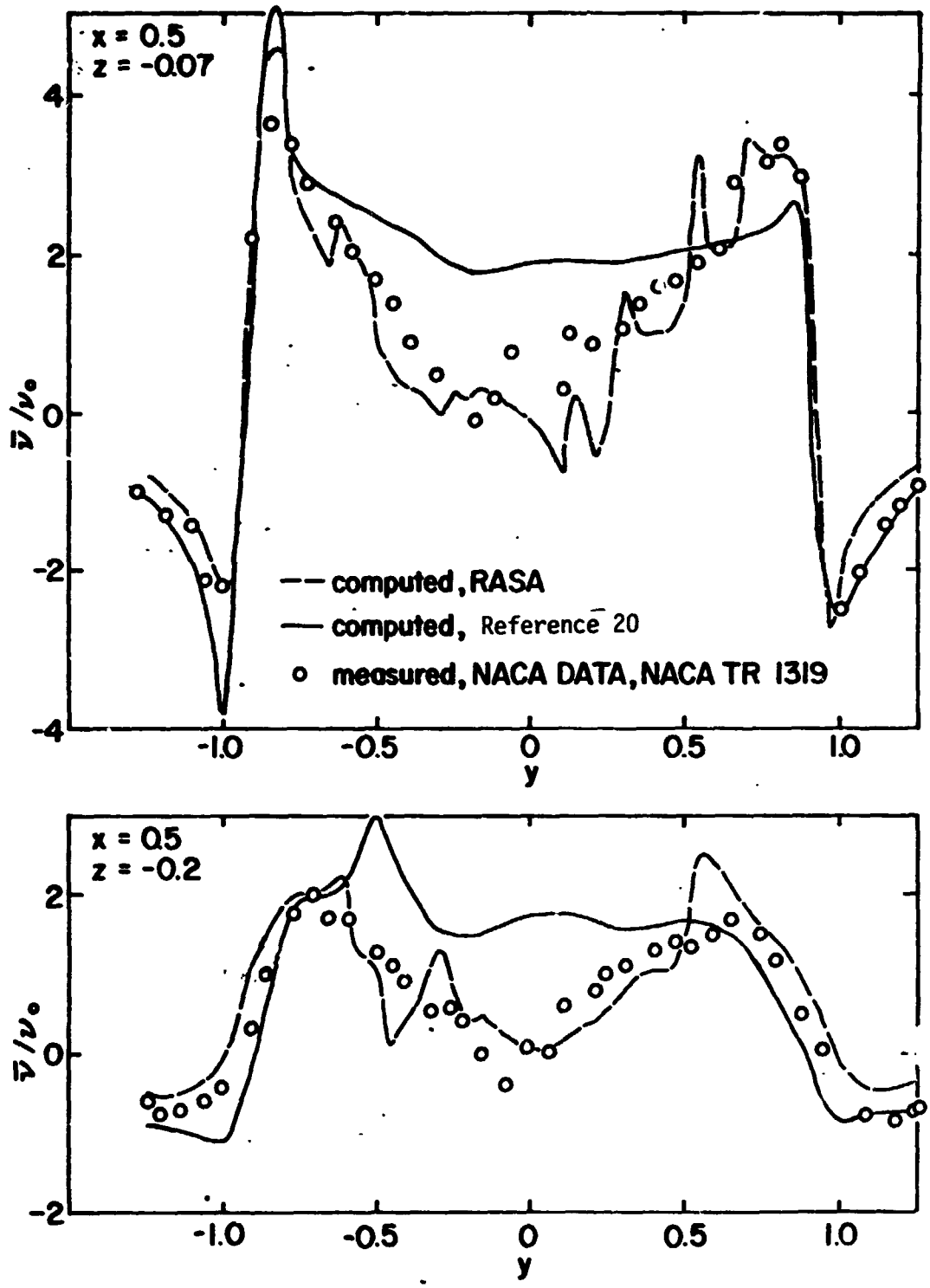

Figure 29. - Comparison of computed and measured induced downwash below the rotor plane, $\mu = 0.14$, $C = 0.00371$, $\chi = 0.5$.

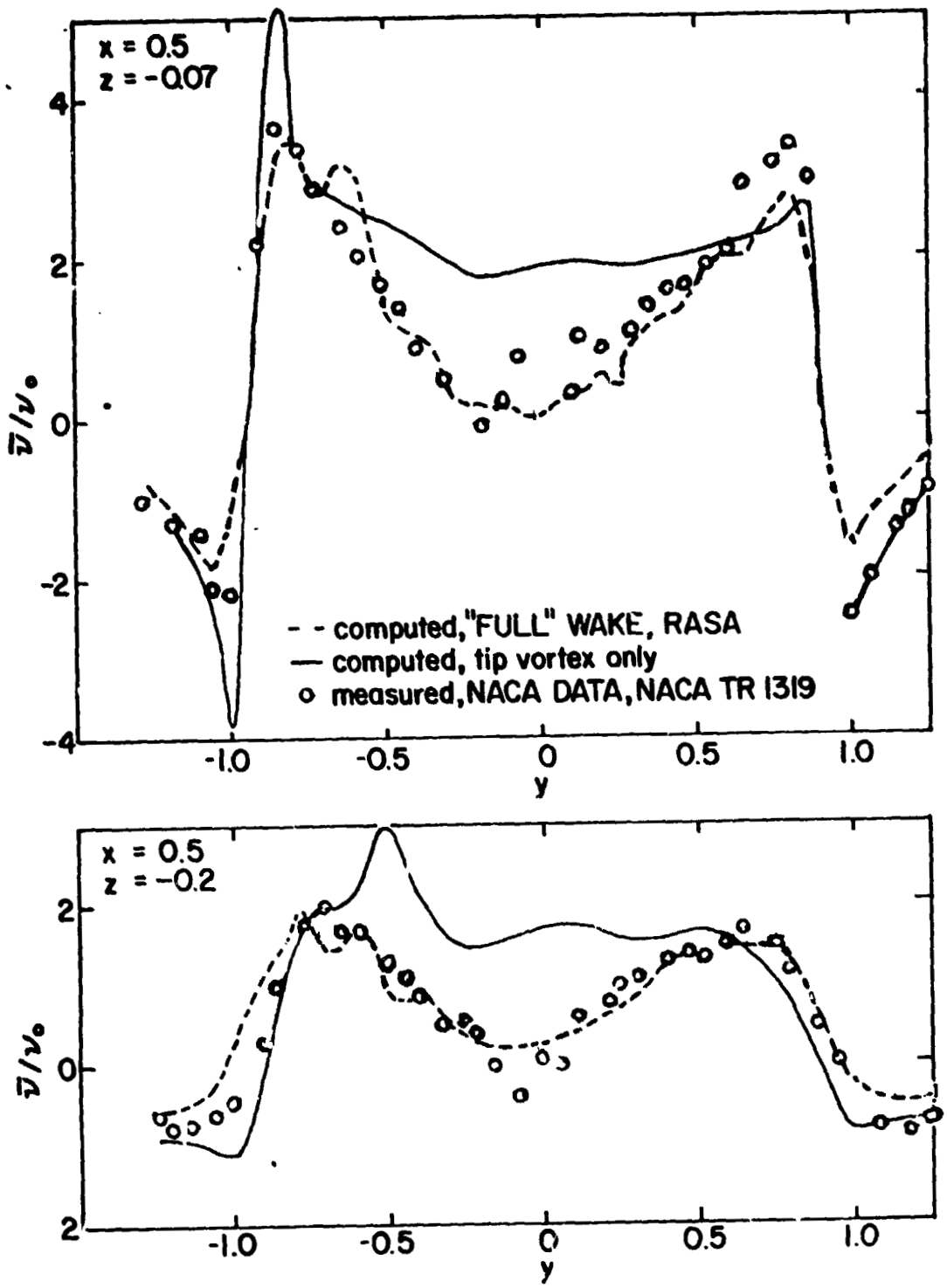

Figure 30. - Comparison of computed and measured induced downwash below the rotor plane, $\mu = 0.14$, $C = 0.00371$, $\chi = 0.5$.

Blade No.	advancing side	retreating side
1	– – –	———
2	——– – ——–	——–·——–

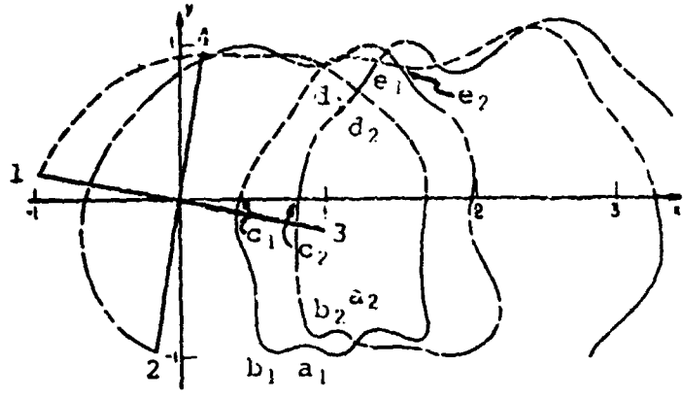

(a) plan view

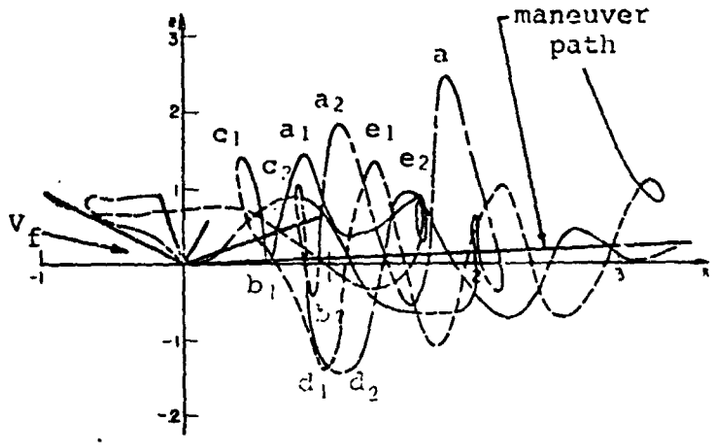

(b) side view

Figure 31. - Sadler's calculated wake shape for H-34 at μ = 0.225 and 1.34 g.

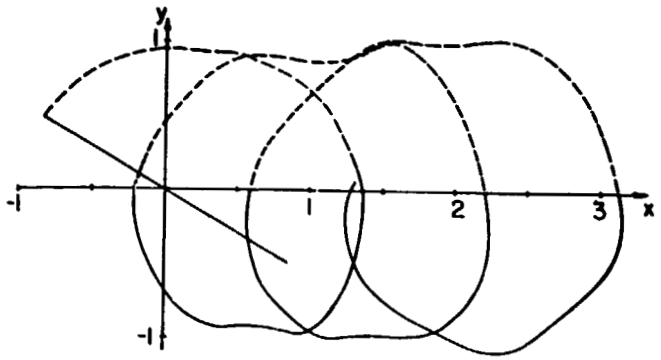

(a) plan view

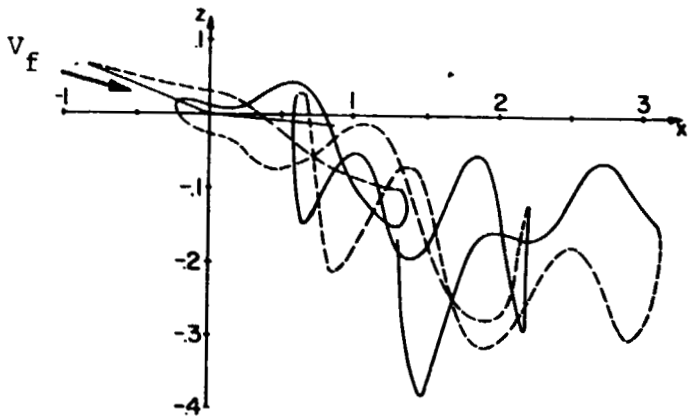

(b) side view

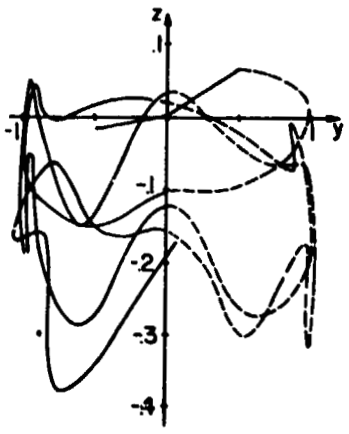

(c) rear view

Figure 32. - Single two-bladed rotor's tip vortex locations, $\mu = 0.141$ $\alpha_s = -5.10$.

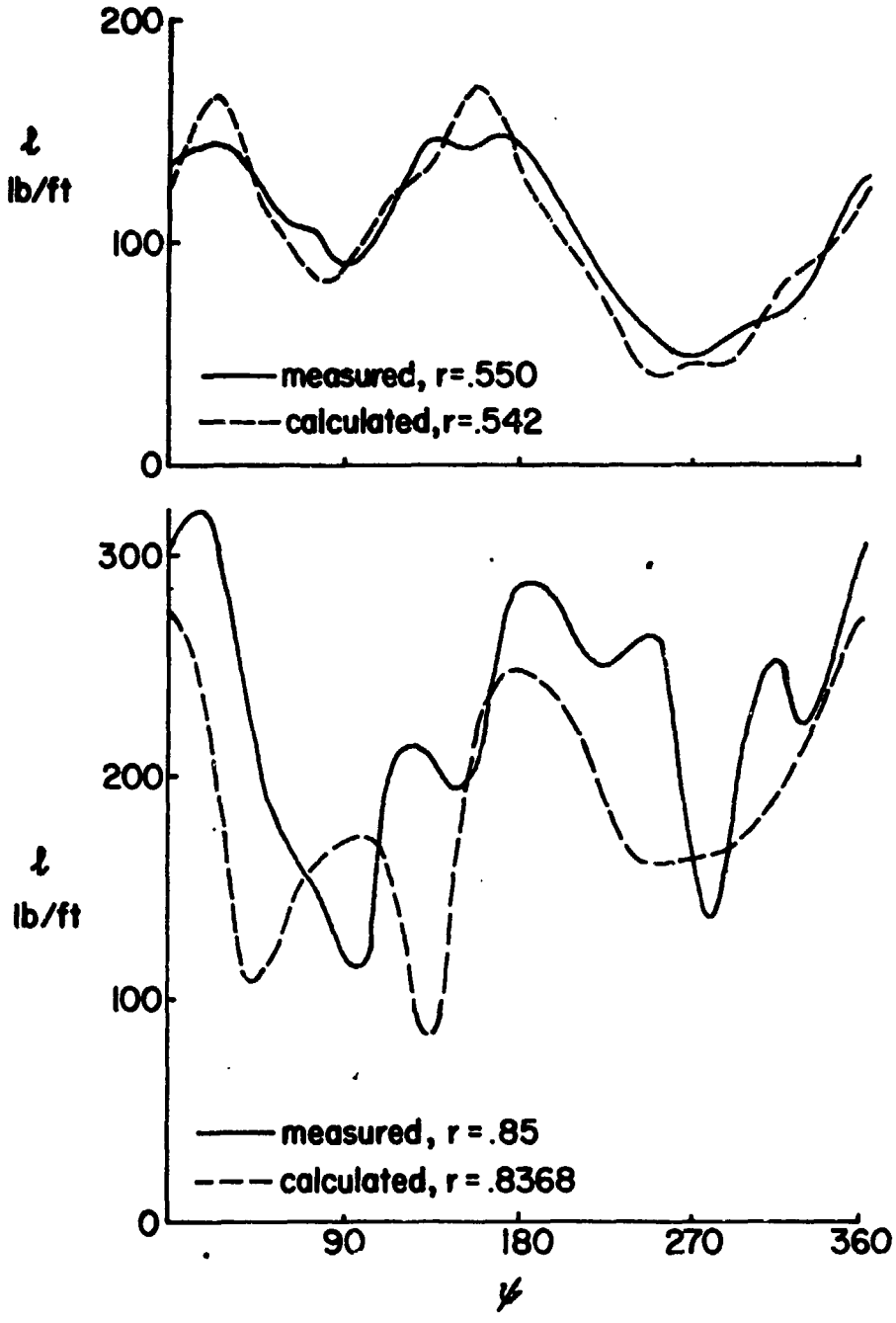

Figure 33. - Blade airloads for H-34 helicopter, lb/ft versus azimuth, $\mu = 0.2$

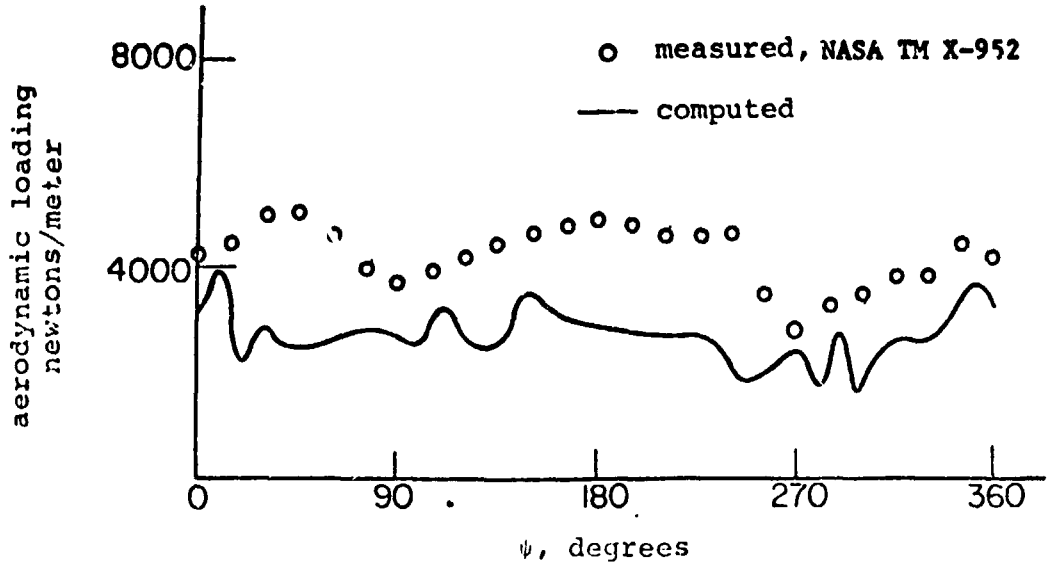

(a) loading at r≃0.75R

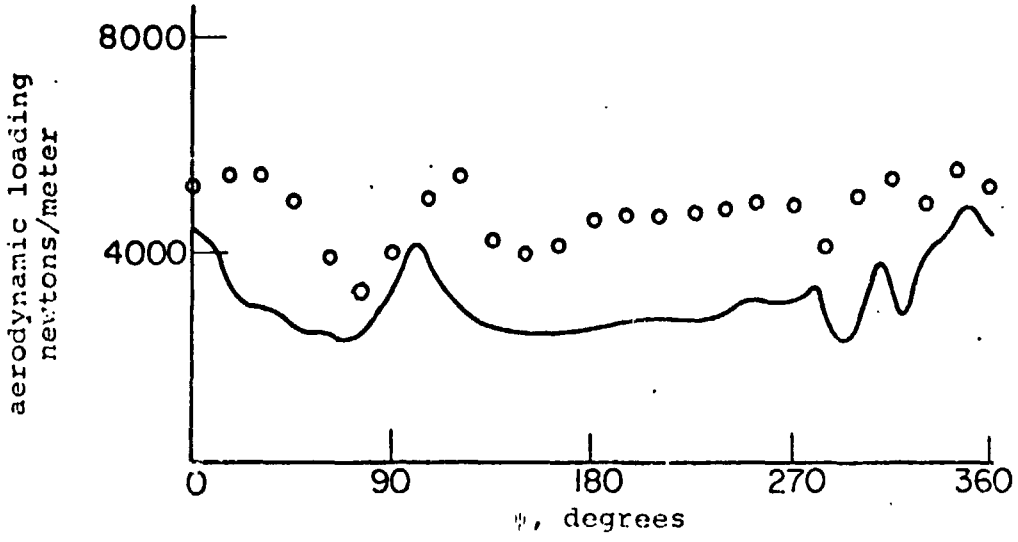

(b) loading at r≃0.90R

Figure 34. - Lifts for H-34 at μ = 0.224 and 1.5 g.

1. Report No.	2. Government Accession No.	3. Recipient's Catalog No.
NASA TM 78741		

4. Title and Subtitle	5. Report Date
A BRIEF SURVEY OF ROTARY WING INDUCED-VELOCITY THEORY	June 1978
	6. Performing Organization Code: 31.600

7 Author(s)	8 Performing Organization Report No.
Harry H. Heyson	

9 Performing Organization Name and Address	10. Work Unit No.
NASA Langley Research Center Hampton, Virginia 23665	516-50-23-01
	11 Contract or Grant No

12 Sponsoring Agency Name and Address	13. Type of Report and Period Covered
National Aeronautics and Space Administration Washington, DC 20546	Technical Memorandum
	14 Sponsoring Agency Code

15 Supplementary Notes

Collateral release of notes prepared for lectures in seminar on Aerodynamics of V/STOL Aircraft and Helicopters, the Pennsylvania State University, University Park, Pennsylvania, July 31-August 4, 1978

16 Abstract

The development of rotary wing induced-velocity theory is traced from its origin as a momentum-theory estimate of average interference, through simple vortex theory, to its present status where it is indispensible in calculating blade loads. Applications to a variety of interference problems is demonstrated. Wherever possible, experimental results are presented to confirm the theory.

17 Key Words (Suggested by Author(s))	18. Distribution Statement
Induced Velocities Helicopters Autogyros Rotor Blade loads Vortex theory	Unclassified - Unlimited Subject Category 02

19 Security Classif (of this report)	20. Security Classif (of this page)	21 No. of Pages	22. Price*
Unclassified	Unclassified	65	$4.50

* For sale by the National Technical Information Service, Springfield Virginia 22161